Research Square

Preprints are preliminary reports that have not undergone peer review.
They should not be considered conclusive, used to inform clinical practice,
or referenced by the media as validated information.

Recognition of BCL-2-interacting killer by GRP78; in silico perspective

Nada R. Abd Alhadiy
Fayoum University
Yasser Y. Ebaid
Fayoum University
Y. Mohammed
Fayoum University
Abdo A. Elfiky
abdo@sci.cu.edu.eg

Cairo University

Article

Keywords: GRP78, BIK, breast cancer, protein-protein docking, MM-GBSA, PCA, molecular dynamics simulation, Apoptosis.

Posted Date: September 10th, 2026

DOI: https://doi.org/10.21203/rs.3.rs-10530713/v1

License: This work is licensed under a Creative Commons Attribution 4.0 International License.
Read Full License

Additional Declarations: No competing interests reported.

Recognition of BCL-2-interacting killer by GRP78; *in silico* perspective

Nada R. Abd Alhadiy [a], Yasser Y. Ebaid [a], Y. Mohammed [a], and Abdo A. Elfiky [b*]

[a] *Physics Department, Faculty of Science, Fayoum University, Fayoum, Egypt*

[b] *Biophysics Department, Faculty of Science, Cairo University, Giza 12613, Egypt*

***Corresponding author**

Prof. Dr. Abdo A. Elfiky, *Ph.D.*

Biophysics Department, Faculty of Science, Cairo University, Giza 12613, Egypt.

Email: abdo@sci.cu.edu.eg

Phone: +201003260523

Abstract

Recent studies have shown that estrogen starvation-induced apoptosis in breast cancer cells requires BIK, a pro-apoptotic BH3-only protein located primarily at the endoplasmic reticulum (ER). However, glucose-regulated protein 78 (GRP78) is critical for endoplasmic reticulum stress and has been observed to be overexpressed in breast cancer cases due to its association with endocrine resistance and evasion from apoptosis through negation of BCL-2 interacting killer (BIK) that induces apoptosis. Characterization of the molecular mechanism behind the GRP78-BIK interactions will aid in designing specific therapeutics. This Study uses a multi-level computational protocol to study the interactions between GRP78 and two different regions of BIK: R1 (C50-C63) and the extended region R2 (C50-C133). Analysis involved docking using HADDOCK, 100 ns molecular dynamics (MD) simulations with NAMD/CHARMM36, RMSD, RMSF, RoG, H-bond, MM-GBSA binding free energy calculations, per-residue decomposition, PCA, and DCCM analysis. The results obtained from the MM-GBSA calculations showed a higher binding energy for the R2 complex (ΔG bind =-50.92 ±12.19 kcal/mol) than for R1(ΔG bind =-31.54±15.90 kcal/mol). Per-residue energy decomposition indicated that the energetic contribution of ARG439 was significant (-10.34 kcal/mol). Hydrogen-bond analysis indicated a salt bridge between ARG439 and ASP95 with 98% occupancy. The PCA and DCCM analyses showed that R2 enables a "dynamic interface," producing a synchronized functional structure and enhanced stability of the GRP78 substrate-binding domain compared with the R1 motif. In

conclusion, this study provides a computational framework that identifies R2 as the primary binding determinant of the GRP78-BIK complex. While these in silico results suggest a promising molecular target in the ARG439 cluster, further biochemical assays are required to validate these interactions and their functional implications for therapeutic resistance. Our observations have led to a pioneering dual-anchor mechanism for the GRP78-BIK complex, in which R1 acts as a recognition anchor and R2 as a stabilizing anchor. This precise molecular architecture has paved the way towards designing a therapeutic approach, in which the ARG439 hotspot cluster can be targeted to release BIK, thereby facilitating apoptosis induction.

Keywords

GRP78, BIK, breast cancer, protein-protein docking, MM-GBSA, PCA, molecular dynamics simulation, Apoptosis.

1. Introduction

Breast cancer continues to be one of the major problems in oncology, being responsible for many cancer-associated mortalities among females [1]. The clinical treatment of this malignancy is hampered by the extensive pathologic heterogeneity and aggressiveness of this type of neoplasm[2][3]. Thus, elucidation of cellular mechanisms, especially the crosstalk between protein-stress pathways and apoptosis, has acquired special importance to identify resistance mechanisms to therapy. An important component of this crosstalk is the GRP78 and BCL-2 interacting killer (BIK), which acts as the key regulatory pathway determining the fate of breast cancer cells. Indeed, GRP78 has been experimentally demonstrated to physically bind BIK and inhibit BIK-induced apoptosis in breast cancer cells, and importantly, this interaction does not require the BH3 domain of BIK, suggesting that GRP78 recognizes an alternative, non-canonical region of the protein[4]. This BH3-independent interaction prompted the current computational search for the specific BIK region mediating GRP78 recognition. BIK, a pro-apoptotic protein from the BCL-2 family, plays a key role in the process of the intrinsic mitochondrial pathway [5].

Recent studies have revealed the importance of this protein in the pathogenesis and aggressiveness of breast cancer[6]. The primary site of localization for BIK is the endoplasmic reticulum (ER). It helps move calcium ions and change the shape of the mitochondrial cristae, which leads to the release of cytochrome c and cell death. Normally, BIK is known to be a tumor suppressor. However, in several types of cancer, such as ovarian, gastric, liver, prostate, and colon cancers, BIK activity is often impaired due to genetic abnormalities or DNA methylation, resulting in resistance to apoptosis and uncontrolled proliferation[7]. Despite the general understanding that BIK levels are low in most tumors, its expression can sometimes be increased in some subgroups of breast cancer and non-small cell lung carcinoma, which surprisingly leads to worse patient outcomes[8]. It also plays an important part in regulating autophagy in MDA-MB-231 cells, underscoring the multidimensional role that it has in tumor development [9].

Under physiological stress, the upregulation of BIK leads to apoptosis by targeting anti-apoptotic factors such as BCL-2 and BCL-XL[10], [11], [12], thereby promoting mitochondrial outer membrane permeabilization[13], [14]. BIK is commonly inactivated in breast carcinoma through the promoter hypermethylation pathway, decreasing the cell's susceptibility to apoptosis [15], [16]. There is also evidence showing a potential connection

between the expression of BIK mRNA and ERα [17]. On the other hand, there have been reports linking high BIK expression to higher stages of disease and poor survival outcomes.

On the other hand, GRP78, an essential ER chaperone and a major regulator of the UPR, is generally overexpressed in cancerous tissues [18]. Normally, GRP78 helps maintain proteostasis; however, when cancerous tissues are subjected to hypoxia, nutrient deprivation, or drug therapy, GRP78 promotes cell survival [19], [20], [21]. It has been found that GRP78 can bind with pro-apoptotic proteins, including BIK, and deactivate their action so that breast cancer cells withstand extended periods of ER stress [22][23], [24], [25]. The binding between GRP78 and BIK is an essential approach in inhibiting apoptosis and is a rapidly developing field of study.

This study attempts to explore the molecular interactions between BIK and GRP78 in breast cancer using computational methods, including structural modeling, protein-protein docking, and molecular dynamics simulations[26]. The goal is to characterize the binding site and the amino acid residues responsible for such interactions. Using this information, we hope to uncover new drug targets and analyze the effects of this interaction in breast cancer metastasis and therapy resistance [27]. Two structural regions of BIK (C50-C63 and C50-C133) will be considered in this study to determine the minimum length of BIK required to form a stable complex with GRP78. Apart from conventional docking, an integrative computational strategy is adopted that involves per-residue energy decomposition to identify energetic “hot spots” and hydrogen bond occupancy to quantify the stability of interfacial interactions. Moreover, DCCM analysis is applied to analyze the coordinated motion patterns between the components of the complex. The objective of such an extensive study is to develop a comprehensive mechanism that explains the manner in which GRP78 binds with BIK, thus serving as a guide to devise inhibitors that would re-sensitize breast cancer cells to apoptosis.

2. Materials and methods

2.1. BIK's 3D structure prediction

The amino acid sequence of the BIK protein was obtained from the UniProtKB database by accessing ID Q13323. To build an accurate 3D model that would be used for further docking studies and molecular dynamics simulations, three prediction software tools named Phyre2, AlphaFold, and I-TASSER were comparatively analyzed. While Phyre2

adopted a homology-based modeling technique with threading against a library of experimental structures[28], both AlphaFold and I-TASSER implemented sophisticated deep learning and ab initio methods, respectively [29], [30]. Candidate structures were also generated by AlphaFold and I-TASSER; however, following the comparative evaluation detailed in section 3.1, the model produced by Phyre2 was selected for further analysis. Structural optimization was performed on the selected structure using the GalaxyRefine server, while its stereochemistry was validated using MolProbity to ascertain the quality and correctness of the structure[31]. The optimized full-length structure was used to perform site-directed docking studies to analyze the energy interactions between BIK and GRP78. The choice of the target regions (C50-C63 and C50-C133) is based on the similarity in the sequence of Pep42 and BIK, as well as on the shared cysteine-bound, disulfide-constrained architecture described in Section 2.2, which supports the concept that GRP78 interacts with BIK through a similar motif. The site-directed docking was performed using the HADDOCK2.4 web server, utilizing the default scoring functions and empirical parameters optimized for protein-peptide interactions.

The initial structures predicted by Phyre2, AlphaFold, and I-TASSER were first individually evaluated for modelling quality using MolProbity and Ramachandran plots in an effort to guarantee a rigorous and reproducible model selection process. The first three models were individually submitted to the GalaxyRefine server, which delivered five refined candidate structures to each tool (15 candidate models in total). Each of the 15 refined PDB models was then reassessed by MolProbity, and its Ramachandran plot was recalculated. For each tool, the best candidate was identified by comparing the five refined models obtained from the tool based on the number of Ramachandran outliers and overall stereochemical quality. The three resulting best models (one for each tool) were then compared to each other to guide the final selection, as detailed in section 3.1.

2.2 Comparative Sequence and Physicochemical Analysis of Pep42 and BIK Regions

The primary structure of the BIK protein, which is a 160-amino acid-long peptide chain with a unique transmembrane (TM) domain, was obtained from the UniProt database [32], [33]. By virtue of the observed similarities in the primary structure of the BIK protein and the cyclic peptide, two particular regions of the BIK protein, namely R1 (amino acids 50–63) and R2 (amino acids 50-133), were recognized to have the potential to be a GRP78-binding motif. The boundaries of R1 and R2 were determined from the three cysteines (Cys50, Cys63, and Cys133) of BIK, which are the only cysteines found within the 160-

amino acid chain. The rationale behind such a choice of boundary can be seen in the structure of the disulfide-bonded circular peptide Pep42 (CTVALPGGYVRVC), where there is an intramolecular disulfide bond between the N-terminal and C-terminal cysteines of this peptide necessary for the selective binding to GRP78 [34]. Thus, setting R1 and R2 in the same way as Pep42 allows comparison on a structural level, not only at the sequence level, which has precedence in recent literature [35].To calculate the level of identity in sequences, pairwise sequence alignments between R1/R2 domains and Pep42 were done using the Clustal Omega server by EMBL-EBI under default parameters[36]. Apart from that, the basic physicochemical properties of R1 and R2 were assessed utilizing the ExPASy ProtParam tool to characterize these structures better. Some of the basic calculations carried out include the Grand Average of Hydropathicity (GRAVY), theoretical isoelectric point (pl), among others [30][37].

2.3 Molecular docking and molecular dynamics (MD) simulation protocol for BIK and GRP78

In order to examine the conformational dynamics and structural stability of GRP78-BIK complex formation, preliminary complex structures were created using a protein-protein docking approach with the HADDOCK 2.4 web server. During the docking process, the SBDβ region of GRP78 was considered as a receptor, while two BIK peptides (R1 and R2) were used as ligands. Docking poses with the highest HADDOCK scores and clusters were chosen for further simulations to assess dynamic differences and binding characteristics of the two regions towards GRP78. The molecular systems (GRP78 protein, BIK peptides, and their docking complex – generated through HADDOCK 2.4) were all prepared using the CHARMM-GUI web server[38], [39], [40], [41]. Solvation of the molecular systems took place within a rectangular box using the TIP3P water model while they were ionized with a 0.154 M NaCl concentration. All MDS simulation runs were performed using the NAMD 2.14 engine by employing the CHARMM36 parameter set. In order to stabilize the initial structures, a 5,000-step energy minimization procedure was performed based on the steepest descent technique [31][35]. Then, all systems were equilibrated in both NVT (number of particles, volume, and temperature constant) and NPT (number of particles, pressure, and temperature constant) ensembles. During the production phase, the temperature of the simulated systems was set at 310 K, while the pressure was maintained at 1atm using Langevin dynamics and the Nose-Hoover Langevin piston methods, respectively. A cutoff of 12 Å was applied for van der Waals and short-range

electrostatic interactions, with a switching function starting at 10 Å. Long-range electrostatic interactions were computed using the Particle Mesh Ewald (PME) method.

The total time for which the simulations have been performed is 100ns for each system, resulting in the generation of 1,000 frames from trajectories for each protein-ligand complex. Post-processing analysis of the output files from the simulations was carried out using in-house scripts within the Visual Molecular Dynamics software version 1.9.3[42], [43], [44]. Structural properties like RMSD, RMSF, RoG, SASA, and H-bonds between intermolecular complexes were evaluated. In order to increase the accuracy of the analysis, the trajectories obtained were classified through UCSF Chimera software. Five frames that represent the most populated clusters from each complex were extracted. These snapshots were used for docking refinement and calculating the binding free energy, thus guaranteeing the proper representation of all the dynamic forms present within the GRP78-BIK complex[45]. Furthermore, Principal Component Analysis (PCA) was performed over the entire 100ns simulation trajectory to capture the essential collective motions of the complexes. Based on the top two principal components (PC1 and PC2), the Free Energy Landscape (FEL) was constructed to map the thermodynamic stability and identify the low-energy conformational basins (global minima) of the GRP78-BIK interaction profiles.

2.4 Molecular docking-based prediction of GRP78 binding modes

In order to analyze the binding mechanisms between BIK and GRP78, the protein-peptide docking experiments were performed using the HADDOCK 2.4 software. Specifically, the GRP78 receptor structure was prepared on the basis of the corresponding crystal structure (PDB ID: 6ASY, Chain A) with all water molecules and heteroatoms stripped off. To take into account the possible flexibility of peptides during the process, structural clusters representing different conformations of the BIK peptide from its 100 ns trajectory were chosen as initial dockings.

In this case, the interface for BIK and GRP78 proteins was formed by defining both R1 and R2 peptides as active. For GRP78, the binding interface was confined to residues that form SBDβ: I426, T428, V429, V432, T434, F451, S452, V457, and I459[38], [46]. To determine the binding energy for each complex, the PRODIGY (Protein Binding Energy Prediction) approach [47], [48] was used. For detailed analysis of interaction landscapes between BIK and GRP78 complexes, the Protein-Ligand Interaction Profiler (PLIP)[49]was

applied. Finally, structural visualization and high-resolution graphical representations were generated using PyMOL and BIOVIA Discovery Studio [50].

2.5 Thermodynamic evaluation of binding affinity via MM-GBSA calculations.

To investigate the thermodynamics of affinity between GRP78 and BIK proteins, the MM-GBSA technique was applied [51]. Even though the initial MD simulations were performed with the use of the NAMD package and CHARMM36 force field, topology and trajectory files were prepared to work with GROMACS-based gmx_MMPBSA software. This was done with the help of the cpptraj tool and specific scripts written for this purpose.

In order to obtain representative conformations, the entire 100ns production trajectory of each system was selected. For these time frames, 1000 evenly spaced frames were taken for energy calculations. Total binding free energy was calculated based on bonded and non-bonded internal energies, electrostatic energy, and the polar contribution to the solvation free energy (estimated by the Generalized Born approximation). Furthermore, non-polar solvation effects were computed based on the solvent-accessible surface area (SASA). The Generalized Born model developed by Onufriev *et al.* (GB^{OBC1}, igb=2) was adopted with default empirical parameters, using solvent and solute dielectric constants set to 80 and 1, respectively. As is commonly done in analogous computational analyses, the entropy contribution was neglected due to significant additional computing costs and uncertainties in estimating its value. To verify this choice, the entropy contribution was additionally estimated using the interaction entropy (IE) and second-order cumulant (C2) approximations implemented in gmx_MMPBSA, and the outcome of this test is reported in section3.4.

The specific molecular factors behind the interaction were further investigated via energy decomposition analysis at the level of individual residues, using the same gmx_MMPBSA tool. This method provides a way of decomposing the total energy of the complex formation into smaller components associated with each residue. Comparing the energy decomposition results between R1 and R2 systems allowed estimating the stabilizing contribution of the surrounding residues from the R2 structure, which contributed to the increased binding affinity to GRP78. The free binding energy ($\Delta G_{binding}$) of each model was determined according to the equation:

$$\Delta G_{binding} = G_{complex} - (G_{receptor} + G_{ligand})$$

In this equation, Greceptor is the independent thermodynamic state of the receptor alone, G_{ligand} refers to the energy of the unbound molecule, while $G_{complex}$ indicates the total energy sum of the complexes [52]. Ultimately, these numerical calculations effectively complement our prior dynamic structural observations. They supply a robust quantitative framework for assessing molecular affinity. The individual energy components were further evaluated using the following standard equation:

$$\Delta G_{binding} = \Delta E_{MM} + \Delta G_{solc} - T\Delta S$$

$$\Delta E_{MM} = \Delta E_{int} + \Delta E_{elec} + \Delta E_{vdw}$$

$$\Delta G_{solv} = \Delta G_{GB} + \Delta G_{SA}$$

where ΔE_{MM} is the gas-phase molecular mechanics energy (encompassing internal ΔE_{int}, electrostatic ΔE_{elec}, and van der Waals ΔE_{vdw} terms), ΔG_{solv} is the solvation free energy (divided into polar ΔG_{GB} and non-polar ΔG_{SA} contributions), and $-T\Delta S$ represents the conformational entropy. Ultimately, these numerical calculations effectively complement our prior dynamic structural observations. They supply a robust quantitative framework for assessing molecular affinity.

2.6 Principal component analysis of conformational dynamics in the GRP78–BIK complex

In order to investigate the major collective motions and flexibility of the assembled structures of GRP78–BIK complexes, PCA was conducted over the entire 100 ns production trajectory to capture the essential collective motions of the complexes. The NAMD trajectory files were converted and processed using Bio3D and GROMACS analysis tools.

Before constructing the covariance matrix, the global translations and rotations were removed by performing a least-squares fit of the protein atoms onto the reference structure. In order to obtain pure conformational motions, it is vital to align the trajectory using this alignment process. Using the gmx make_ndx command, an index file will be made, designating the backbone atoms as the selection.

For the calculation of the covariance matrix and obtaining the eigenvectors and eigenvalues for the motion, the gmx covar command was used. The motion in the direction defined by the eigenvector with the highest eigenvalue is considered the most dominant movement. Using the gmx anaeig module, projection was done of the simulated trajectory on the first two principal components (PC1 and PC2)[53][54]. Subsequently, the Free Energy Landscape (FEL) was constructed from the joint probability distribution of PC1 and

PC2 to map the thermodynamic stability and locate the low-energy conformational basins of the complexes. The FEL was calculated using the standard Boltzmann relationship:

$$F(X)= -k_BTlnP(X)$$

where k_B is the Boltzmann constant, T is the simulation temperature (310K), and P(X) is the probability distribution of the system along the PC1 and PC2 coordinate axes.

2.7 Interfacial stability and dynamic coordination analysis

In order to evaluate the interfacial stability of the interaction between the BIK segments (R1 and R2) and the GRP78 chaperone, the hydrogen bond occupancy was analyzed during the entire 100 ns production run. According to the standard criteria of geometry, a hydrogen bond was considered when the donor-acceptor distance was 3.5 Å or less, with maximum deviation from linear orientation less than 30° [55]. Occupancy was calculated as the percentage of the total simulation time and served as an estimate of the persistence and stability of individual interactions, allowing the identification of the interaction that ensures the stability of the complex. Hydrogen bond and salt bridge occupancies were calculated directly on the solvated NAMD system in VMD. Note that a +1000 residue-numbering offset was intentionally introduced for the GRP78 chain during system preparation for docking to avoid any residue numbering conflicts with the BIK peptide (residues 1-160) when the two chains were merged into a single docked complex. Consequently, GRP78 (segment PROB) has this offset residue numbering from the docked complex (residues 1024-1629). The original numbering does not correspond directly to the standard UniProt sequence numbering, since the resolved GRP78 construct used in this study starts at UniProt residue 24. To ensure full internal consistency and concordance with UniProt, all GRP78 residue numbers presented throughout this manuscript (including hydrogen-bond/salt-bridge partners and the per-residue MM-GBSA energy decomposition results, Section 2.5) have thus been normalized by subtracting 1000 from the original docked-complex residue number (e.g., the salt-bridge donor originally labeled ARG1439 is reported throughout this manuscript as ARG439). The sequential residue numbering generated separately during system preparation in GROMACS/gmx_MMPBSA was cross-validated against this standardized numbering and corrected accordingly (see Table 4). This correction affected only the residue-number labels used to identify each residue; the underlying MM-GBSA energy values themselves, computed independently for each residue position, were not altered by this renumbering.

Moreover, the overall coordination and mechanical coupling of the studied complexes were investigated using the dynamic cross-correlation matrix (DCCM) method [56]. Using the Bio3D module of the R software environment, the cross-correlation coefficients (C_{ij}) for the atomic displacements of C^{α} atoms were determined. Coefficients C_{ij} vary from -1 (completely anticorrelated atoms) to +1 (completely correlated). C_{ij} was depicted as a heat map to identify areas of synchronized motions. This method allowed us to elucidate how the flanking residues of the R2 region affect the dynamics and stability of the binding site of the substrate in comparison to the R1 motif [57], [58].

3. Results and Discussion

The sustained upregulation of GRP78 (BiP) is a hallmark among many types of cancers, showing high frequency especially in breast carcinoma, where it predominantly determines the drug resistance to anti-estrogen treatment. Acting as a major chaperone of the Hsp70 family residing in the ER, GRP78 acts as an essential regulator in the Unfolded Protein Response (UPR) and confers proteotoxic stress-induced cell survival[59], [60][4]. A considerable number of observations made both in vitro and on biopsy samples demonstrate increased resistance to chemotherapy in association with elevated levels of GRP78 in breast cancer patients [61], [62].

At the center of this defense mechanism is the inhibition of BIK, which is one of the major mediators of pro-apoptosis via BH3-containing proteins. Studies conducted on the role of GRP78 in breast carcinomas have proven that the overexpression of GRP78 successfully antagonizes the activity of BIK, consequently providing protection against apoptosis induced by anti-estrogens[4], [5]. Therefore, the suppression of GRP78 is expected to result in significantly higher susceptibility to hormone-based therapy in tumor cells. Considering the close proximity and interaction between BIK and GRP78 within common cellular compartments, further research into the location of BIK and GRP78 is crucial[4].

This makes BIK an attractive target for potential therapies, since methods of restoring its expression may be employed to counter the effects caused by the inhibition of apoptosis. Inhibitors of GRP78, proteasome inhibitors, and doxorubicin, all of which have shown success in restoring BIK expression, could represent potential treatment avenues. [5]. Identifying the particular regions in which BIK and GRP78 overlap, as well as the unique

molecular components involved in both autophagy and apoptosis cascades, is of crucial importance.

3.1. Comparative sequence profiling and conformational analysis of Pep42 and BIK (R1/R2) peptides

Based on results shown in Table 2 and Figure 1, it can be inferred that there is a high degree of sequence homology between the selected sequences of BIK and the Pep42 cyclic peptide. Namely, residues R1 (50-63) and R2 (50-133) have sequence similarities equal to 23.08% and 25.00%, respectively. Considering that Pep42 is known to act as a specific ligand of cell surface GRP78 receptors in cancerous cells[63]. These similarity values provide a structural explanation for the capacity of the selected sequences to recognize GRP78. In addition, comparative physicochemical properties of these peptides indicate that the GRAVY value of Pep42 is 1.1, while for BIK R1 and R2 are 0.78 and 0.07, respectively. High hydrophobicity of BIK R1, similar to Pep42, suggests its contribution to hydrophobic contacts between BIK and GRP78 receptors. In addition to sequence similarity, R1 and R2 peptides also possess a secondary structural element common to Pep42, as depicted in Figure 1 below: both R1 and R2, as well as Pep42, possess cysteine bonds at their N- and C-termini (Cys50-Cys63 for R1, Cys50-Cys133 for R2, and Cys1-Cys13 for Pep42). This is characteristic of the secondary disulfide-stabilized cyclic structure that mediates the specificity of Pep42 toward GRP78 [34]. It adds another dimension of evidence for choosing R1 and R2 as GRP78 binding sites regardless of their sequence similarities. After performing the sequence-based analysis, the 3D structure of BIK was modeled with Phyre2 and further optimized using the GalaxyRefine server. In order to verify the correctness of the model before further simulation studies, the stereochemistry of the structure was analyzed through MolProbity. The optimized model structure (Figure 2A) was found to be very consistent based on the Ramachandran plot (Figure 2B), where 89.2% (141 out of 158 residues) fall within the most favorable region, and 98.1% (155 out of 158 residues) lie within the allowed region.

To justify the choice of the Phyre2-derived model over AlphaFold and I-TASSER, the initial structure generated by each of the three tools was submitted to the GalaxyRefine server, resulting in five refined candidate models per tool (15 candidate models in total). For each of the 15 models, the individual MolProbity evaluation identified the best candidate (lowest MolProbity score, lowest clashscore, and fewest Ramachandran/rotamer outliers among the 5 candidates from each tool). The best model for each tool was AlphaFold

(MolProbity score = 1.34, 98th percentile), Phyre2 (MolProbity score = 2.17-2.20, 64th-66th percentile), and I-TASSER (MolProbity score = 2.84, 29th percentile). The AlphaFold model had a numerically better all-atom geometry score, but the per-residue confidence (pLDDT) analysis revealed an average pLDDT of 62.5 (low) with ~60% of the sequence in the low-to-very-low confidence range and a very disordered loop conformation covering residues around the R2 motif (~120–145). This is in line with the known intrinsically disordered nature of the BIK N-terminal region. Since a stable, well-folded conformation of this region was needed for reliable docking and MD simulation of the GRP78–BIK interface, the Phyre2 model generated by homology-based threading against experimentally resolved templates was used instead to provide a more compact and biologically representative fold for this segment. The final model (Model 2) was selected from five candidate models generated by Phyre2 based on its ranking by the GalaxyRefine server and its side-chain packing quality (98.60% favored rotamers, 1.40% poor rotamers, and the lowest Cβ-deviation and CaBLAM outlier counts among the five candidates), qualities that are particularly pertinent to interfacial hydrogen-bonding and hydrophobic contact formation in the ensuing docking and MM-GBSA analyses. Another Phyre2 candidate (Model 3) was observed to have a marginally better backbone Ramachandran distribution (Z-score −2.83 versus −2.97) and a better overall MolProbity score (2.17 versus 2.20); however, this difference was small (ΔMolProbity = 0.03) and did not outweigh the better side-chain quality of Model 2 for this study.

Table 1: Comparison of the best-performing refined model (selected from among five GalaxyRefine candidates) obtained from each of the three structure-prediction tools.

Tool	Best Model	Clashscore	MolProbity Score (Percentile)	Favored Rotamers	Ramachandran Favored	Cβ Deviations	CaBLAM Outliers
AlphaFold	Model2	6.22	1.34 (98th)	98.60%	99.37%	0.00%	0.00%
Phyre2	Model2	10.11	2.20 (64th)	98.60%	89.60%	5.26%	9.60%
I-TASSER	Model4	33.83	2.84 (29th)	96.50%	81.01%	15.79%	8.33%

Table 2: Comparative Analysis of Pep42 and BIK Regions R1 (C50–C63) and R2 (C50–C133)

BIK region	Sequence Identity %	GRAVY	Sequence length
R1: C50-C63	23.08%	0.786	13
R2: C50-C133	25.00%	0.07	83
Pep42	100.00%	1.1	13

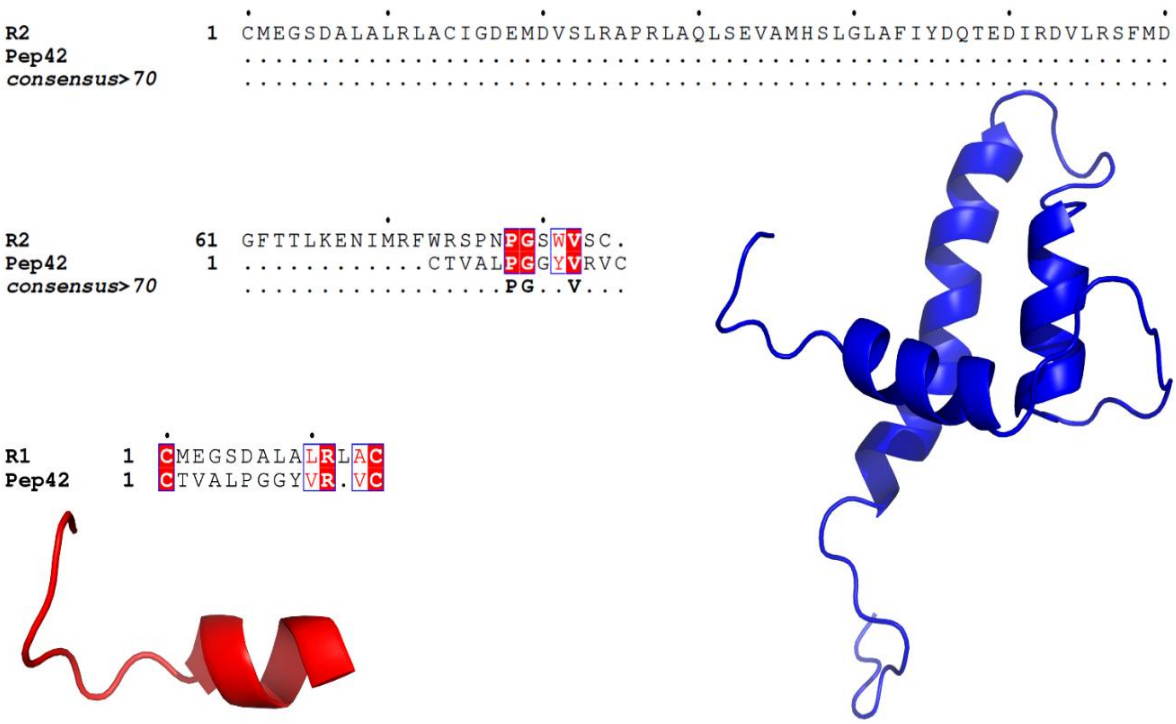


Figure 1 The pairwise sequence alignment of the BIK regions (R1: C50-C63 and R2: C50-C133) with the cyclic peptide Pep42. The alignment was made by Clustal Omega and visualized by ESPript 3.0, while the structures were depicted by PyMOL.

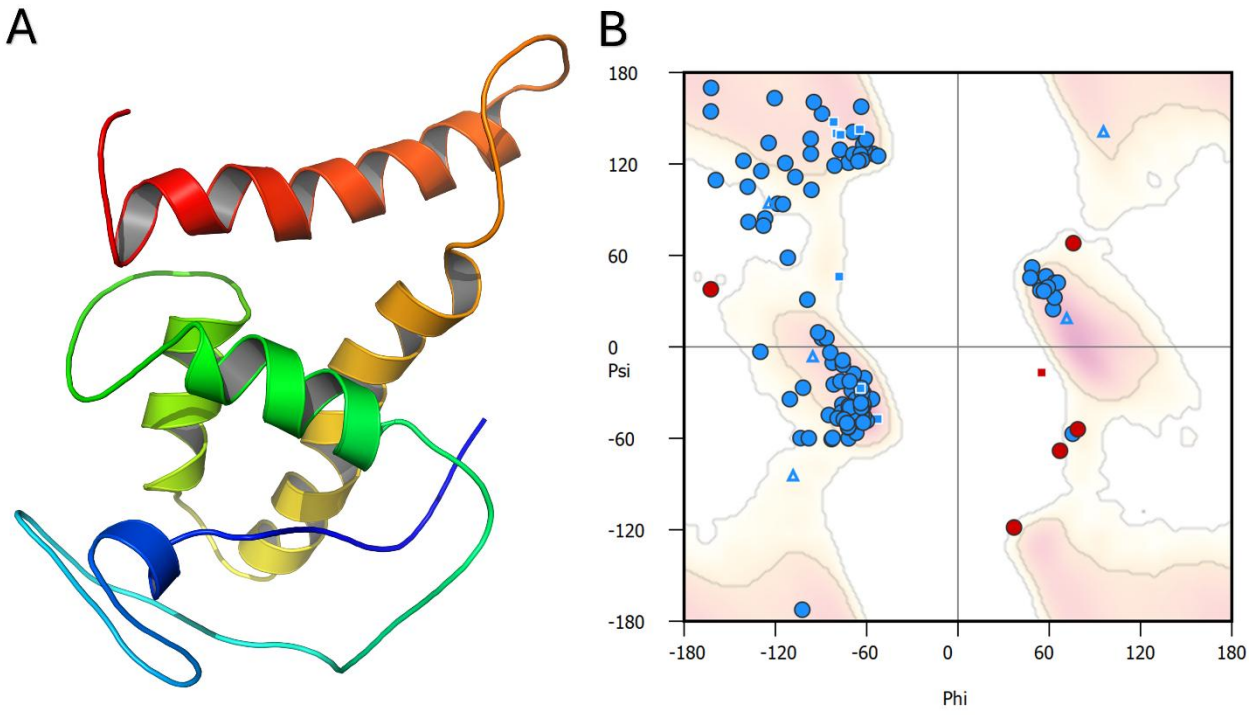


Figure 2 (A) Phyre2 3D structure for the BIK protein, (B) analysis of the Phyre2 model for the BIK protein using a Ramachandran plot

These metrics, combined with the physicochemical profiles detailed in Table 2, validate the BIK model as a robust template for high-resolution molecular modeling and docking studies.

3.2 *Structural Insights into GRP78-BIK Binding Modes at Regions R1 and R2*

To investigate the mechanism of the protein-protein interactions between BIK and GRP78, macromolecular docking was carried out utilizing the HADDOCK 2.4 software package. The docking simulation involved targeting the SBDβ domain of the GRP78 receptor (PDB: 6ASY, Chain A). In particular, the primary interaction pocket of GRP78 receptor was considered in this work, including residues I426, T428, V429, V432, T434, F451, S452, V457, and I459.

To allow for the conformational flexibility of BIK, the five structural clusters identified from the MD simulation trajectories of the BIK protein were used as ligand models in the docking simulation.

The energetic parameters of the complexes generated are provided in Figure 3, showing the mean HADDOCK score and binding affinity (ΔG) values along with their respective standard deviation. Specifically, the R1-GRP78 complex possessed an average HADDOCK score of −53.78 ± 2.82 and a binding affinity of −7.36 ± 1.06 kcal/mol.

Conversely, the R2-GRP78 complex possessed an average HADDOCK score of −30.16 ± 7.56 and a remarkably low binding energy of −11.29 ± 1.63 kcal/mol.

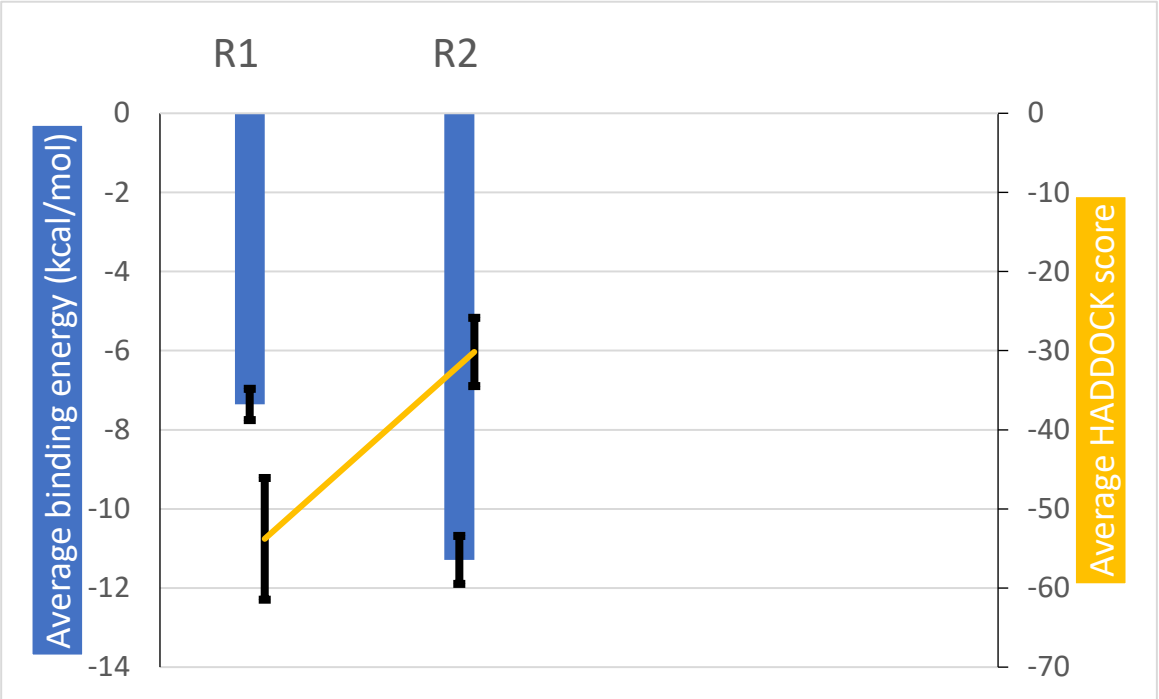


Figure 3 Average docking scores and binding free energies (ΔG) of BIK regions R1 (C50–C63) and R2 (C50–C133) with GRP78, as computed using the HADDOCK v2.4 web server.

This suggests that the energy levels associated with the two peptides are different. It is observed that R1 scores higher in the HADDOCK score, which denotes an improvement in terms of docking geometry and complementarity, while R2 scores better in terms of its thermodynamic energy score. This is evident from the low ΔG value of the R2–GRP78 SBD protein complex. The reason behind such an observation lies in the additional interactions facilitated by the surrounding residues. Overall, the results reveal that both R1 and R2 motifs of BIK can interact effectively with the GRP78 SBD domain.

3.3 *Conformational Dynamics, Stability, and Residual Flexibility (100 ns MDS)*

In order to explore the full range of BIK conformations and binding energy during complex relaxation processes, 100-nanosecond-long MD simulations were performed for the isolated BIK, isolated GRP78, and the GRP78–BIK complexes (termed R1 and R2). It was determined from the analysis of RMSD that the simulated time scale was sufficiently large to provide adequate equilibration of proteins. Further analysis was based on RMSD (Figure 4A), radius of gyration (RoG) (Figure 4B), total intermolecular hydrogen bonds (Figure 4C), and solvent-accessible surface area (SASA) (Figure 4D).

Based on the obtained RMSD trajectories, it is clear that all studied systems were stable within 100 ns of the production run. The average RMSD values (with SD) were found to be 8.4 ± 1.4 Å for BIK, 4.2 ± 1.2 Å for GRP78, 5.9 ± 1.3 Å for the BIK_R1–GRP78 complex, and 4.06 ± 0.75 Å for the BIK_R2–GRP78 complex. Such results confirm the equilibration state for all simulated structures, with R2 showing the highest structural stability. The R2 structure exhibits fewer fluctuations than the other complexes.

Validation using RoG, SASA, and hydrogen-bond analyses has shown that no significant changes in stability occurred. Specifically, the values of SASA were quite stable, averaging around 11,460.1 Å² (BIK), 31,182.5 Å² (GRP78), 41,689.6 Å² (BIK_R1 complex), and 41,465.7 Å² (BIK_R2 complex). In addition, the value of RoG averaged at about 17.3 Å (BIK), 29.6 Å (GRP78), 34.8 Å (BIK_R1 complex), and 33.7 Å (BIK_R2 complex). These data confirm that no significant expansion of the complexes occurred, maintaining a compact fold of protein molecules. Moreover, the intermolecular contact network in the R2 complex was greatly strengthened, and the number of hydrogen bonds reached its highest level, at 197.2 compared to 175.7 in the case of R1. This increase in the hydrogen bonds explains the high level of interaction in the R2 region.

Supplementing the previous observations, Figure 4E provides RMSF values. Average RMSF values for different proteins were calculated as 2.8 ± 1.6 Å (BIK), 2.1 ± 1.1 Å (GRP78), 3.5 ± 1.9 Å (BIK_R1–GRP78), and 2.4 ± 1.6 Å (BIK_R2–GRP78). Based on the analysis of the R1–GRP78 complex (blue color), one can observe an increase in fluctuations in the SBDα region of GRP78. In contrast, the R2–GRP78 complex (green) maintained a stability profile nearly identical to the isolated BIK and GRP78 proteins, suggesting a highly rigid, energetically favorable binding mode that minimizes entropic loss upon association.

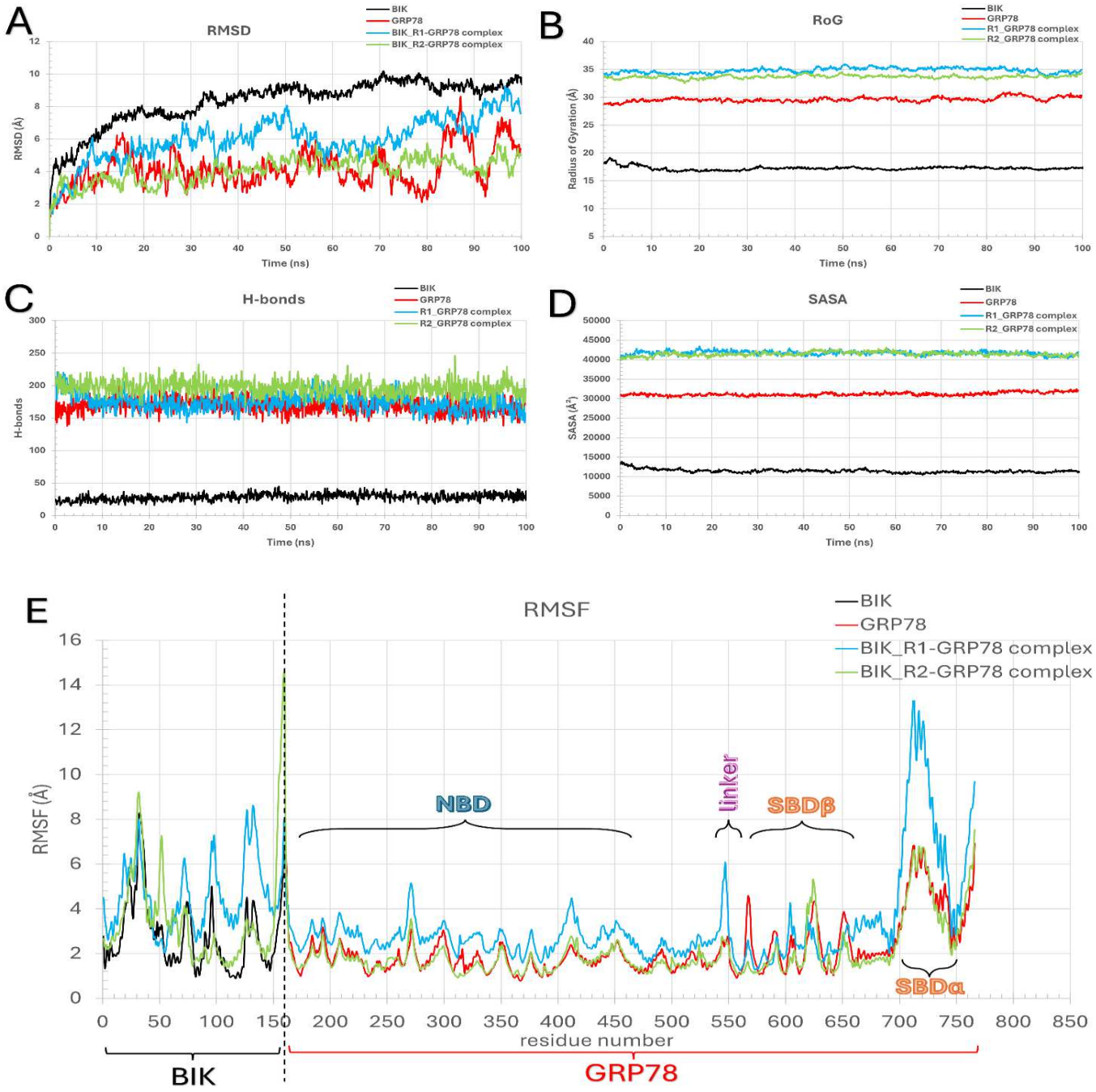


Figure 4 (A) the root mean square displacement (RMSD, Å), (B) radius of gyration (Rg, Å), (C) H-bond and (D) solvent-accessible surface area (SASA, Å²), and (E) Root mean square fluctuation (RMSF, Å) of the proteins during the molecular dynamics (MD) simulation for BIK (black), GRP78 (red), R1_GRP78 complex (blue) and R2_GRP78 complex (green).

3.4 *Thermodynamic Assessment and Per-residue Energy Decomposition of GRP78-BIK Binding*

The calculation of the binding free energies and identification of contributions from individual residues to thermodynamic stability were performed using the MM-GBSA approach combined with the per-residue energy decomposition analysis, using the snapshots

collected during the entire 100ns of the molecular dynamics simulations. As shown in Table 3, the interaction of the GRP78 protein with the BIK_R2 fragment was associated with significantly lower (ΔG_{bind} = −50.92 ± 12.19 kcal/mol) binding free energy than its interaction with the BIK_R1 fragment (ΔG_{bind} = −31.54± 15.90 kcal/mol). Such a difference suggests an increase in the stability of interactions of the GRP78 protein with the extended BIK_R2 fragment. The entropic contribution to binding was further estimated using the Interaction Entropy (IE) and second-order cumulant (C2) approximations. In both approaches, the ΔG_{bind} estimates we obtained were strongly divergent (roughly +100 to +7,300 kcal/mol) and physically unrealistic, instead of a meaningful correction to the enthalpy-based values above. This behavior is a known failure mode of exponential-averaging entropy methods, which fail to converge once the standard deviation of the interaction energy distribution (σIE) exceeds ~15 kJ/mol, and produce unrealistically large entropies once σIE exceeds ~25 kJ/mol [64]. The systems studied here, BIK_R1-GRP78 and BIK_R2-GRP78, showed much larger fluctuations (σ ≈ 330-400 kJ/mol) well outside this convergence limit. This result empirically validates the numerical unreliability of entropy estimation for the systems in question, supporting the use of the enthalpy-dominated ΔG_{bind}. This result provides empirical evidence for the numerical unreliability of entropy estimation for the present systems, supporting the use of the enthalpy-dominated ΔG_{bind} values reported above as relative, comparative measures of binding strength between R1 and R2, rather than as absolute, experimentally comparable quantities.

Table 3: Binding free energy calculations for BIK_R1-GRP78 complexes and the BIK_R2-GRP78 complex via the MM-GBSA method

	ΔG_{bind} (Kcal/mol)	ΔEVDW (Kcal/mol)	ΔE_{EL} (Kcal/mol)	$\Delta GB(E_{GB})$ (Kcal/mol)	$\Delta SA\ (E_{SURF})$ (Kcal/mol)	ΔG_{GAS} (Kcal/mol)	ΔG_{SOLV} (Kcal/mol)
R1_GRP78 complex	-31.54 ±15.90	-63.12 ±9.24	613.95 ±77.66	-572.79 ±72.53	-9.63 ±1.90	550.83 ±79.45	-582.37 ±71.90
R2_GRP78 complex	-50.92 ±12.19	-80.43 ±9.37	433.69 ±93.43	-391.22 ±89.69	-12.97 ±1.42	353.26 ±95.25	-404.19 ±89.02

According to energy decomposition analysis, the van der Waals interactions (ΔE_{vdW}) contribution was larger for the BIK_R2–GRP78 interaction (−80.43 ± 9.37 kcal/mol) than for the BIK_R1–GRP78 one (−63.12 ± 9.24 kcal/mol). The electrostatics contribution (ΔE_{elec}) for the BIK_R2–GRP78 complex (+433.69 ± 93.43 kcal/mol) was different compared to BIK_R1 (613.95 ±77.66 kcal/mol). The increased values of these parameters suggest the altered hydrophobic packing and complementary charge distribution of the BIK fragments bound to GRP78.

The analysis of contributions of different types of solvation energy showed significant differences between the complexes. While the polar solvation energy contribution ΔG_{GB} was (-391.22 ± 89.69 kcal/mol) for BIK_R2 compared to (-572.74 ± 72.53 kcal/mol) for BIK_R1 complexes, the opposite trend was observed for nonpolar solvation energy ΔG_{SA}. The value was −12.97± 1.42 kcal/mol for R2 vs −9.63 ± 1.90 kcal/mol for R1. The total solvation energy (ΔG_{solv}) was estimated to be -404.19 ± 89.02 kcal/mol for R2 and -582.37 ± 71.90 kcal/mol for R1.

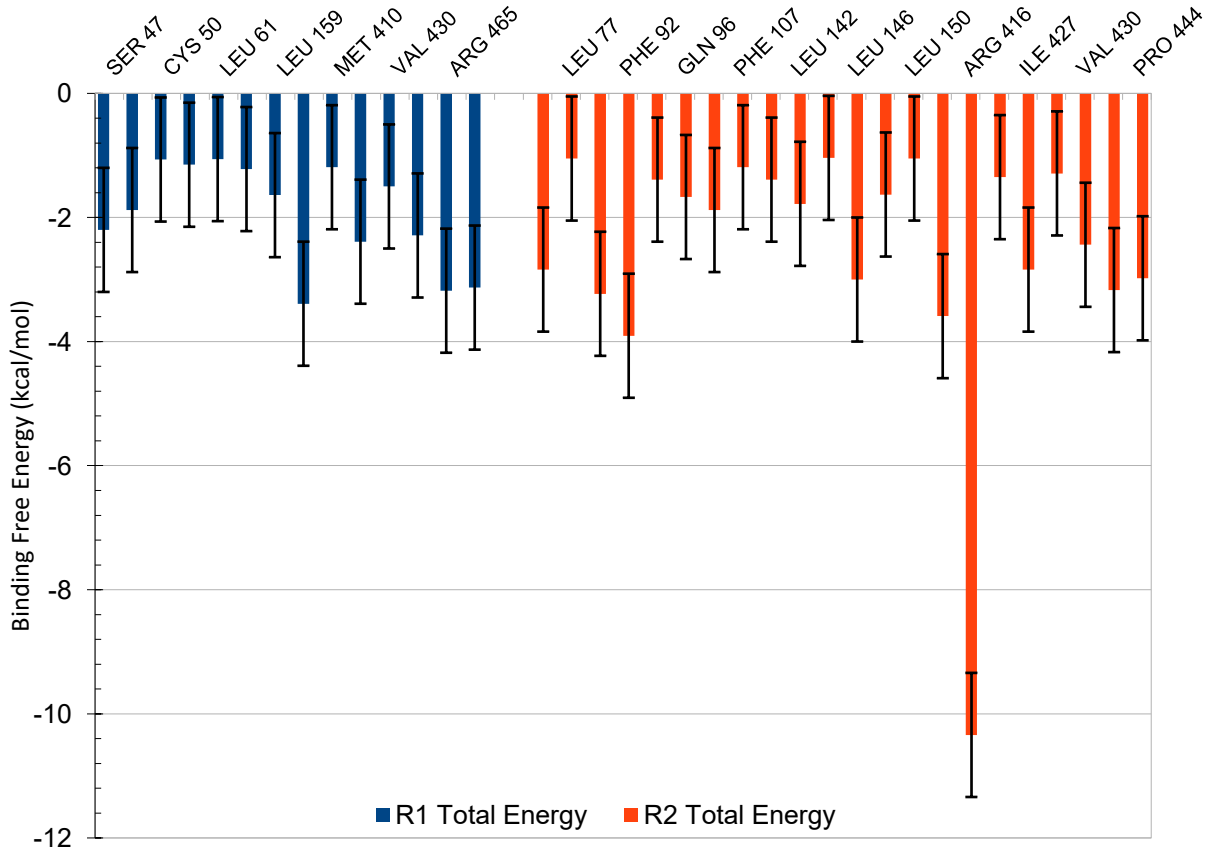


Figure 5: per-residue binding free energy decomposition of GRP78-BIK complexes. Comparative analysis of the energetic contributions of key residues in the R1 (blue) and R2 (orange) binding regions. The vertical axis represents the total binding free energy (ΔG_{bind}) in kcal/mol. Identification of primary "hotspot" residues, where ARG:439 in GRP78 and PHE:92 in BIK exhibit the most significant stabilizing contributions in the R2 complex. The denser and more favorable (negative) energy profile in the R2 region highlights the role of flanking residues as "molecular anchors" that enhance thermodynamic stability and mitigate the polar solvation penalty, providing a structural basis for the high-affinity GRP78–BIK interaction.

The gas-phase interaction energy value ΔG_{gas} proved to be 353.26 ± 95.25 kcal/mol for R2 compared to 550.83± 79.45 kcal/mol for R1. This can be attributed to significant enthalpic effects in both systems that were able to balance the thermodynamic behaviors. As a means of exploring the mechanism behind this thermodynamic behavior, the per-residue energy decomposition was performed in order to determine the role of hotspot residues in driving the interactions between proteins and peptides, as described in Figure 5 and Table 4. It is clear from the results that the excellent binding strength of R2 was due to the existence of highly energetic residues at certain positions on the GRP78 peptide, including ARG:439 and ARG:466, which were associated with energy values of -10.34 kcal/mol and -3.17 kcal/mol, respectively. These residues demonstrated great electrostatic localization, serving as electrostatic anchors that stabilized the binding of the BIK peptide.

Table 4 Per-residue binding free energy decomposition (kcal/mol), electrostatic and van der Waals for the GRP78-BIK complex in Region 1 (R1) and Region 2 (R2) calculated using the MM-GBSA method.

Regions	Residue	Total Energy(kcal/mol)	Electrostatic	Van der Waals
R1	L:A:SER:47	-2.2±11.8	11.73±13.6	-1.5±1.3
	L:A:LEU:48	-1.88±11.8	-0.99±2.99	-2.36±1.56
	L:A:CYS:50	-1.066±8.8	-0.66±4.6	-1.86±0.98
	L:A:ALA:58	-1.15±4.87	-0.72±2.5	-1.18±1.01
	L:A:LEU:61	-1.059±6.69	0.33±2.16	-1.19±1.29
	L:A:LEU:158	-1.22±8.72	-1.14±4.5	-1.4±1.43
	L:A:LEU:159	-1.64±7.02	-1.34±3.65	-1.84±1.35
	R:B:VAL:432	-3.39±8.55	0.35±4.1	-3.5±1.45
	R:B:MET:433	-1.19±8.18	-0.35±5.33	-0.5±2.3
	R:B:LYS:435	-2.39±38.96	-161.24±28.8	-0.11±1.9
	R:B:VAL:453	-1.5±10.36	0.168±6.15	-1.54±1.28
	R:B:LEU:468	-2.29±12.25	0.23±6.64	-2.54±2.19
	R:B:ARG:488	-3.18±31.07	-76.34±22.57	-0.157±1.85
	R:B:VAL:490	-3.13±7.88	-2.66±4.10	-2.68±1.5
R2	L:A:ARG:76	-2.84±28.02	-41.5±19.9	-1.68±2.13
	L:A:LEU:77	-1.05±8.02	0.079±3.85	-1.49±1.53
	L:A:GLN:79	**-3.23±9.64**	**-5.09±5.95**	**-3.45±1.48**
	L:A:PHE:92	**-3.906±6.67**	**-7.61±3.58**	**-2.5±1.36**
	L:A:ILE:93	-1.39±10.77	-2.017±5.42	-1.16±1.68
	L:A:GLN:96	-1.67±9.85	-4.43±6.31	-1.59±1.83
	L:A:VAL:103	-1.88±5.74	0.406±2.59	-1.77±1.42
	L:A:PHE:107	-1.19±5.29	0.06±2.09	-1.48±1.39
	L:A:LEU:114	-1.39±5.3	-0.12±1.97	-1.34±1.42
	L:A:LEU:142	-1.78±5.65	1.208±2.42	-1.85±1.26
	L:A:LEU:143	-1.04±6.94	0.28±3.15	-1.27±1.69
	L:A:LEU:146	-3±7.09	0.62±3	-3.32±1.31
	L:A:PRO:149	-1.63±5.89	-1.19±2.67	-1.5±1.33
	L:A:LEU:150	-1.05±8.58	-0.79±4.41	-1.19±1.9
	R:B:VAL:432	-3.59±8.55	-2.17±4.79	-3.51±1.27
	R:B:ARG:439	-10.34±18.59	-157.68±13.44	2.20±3.24
	R:B:GLN:449	-1.35±7.66	-3.05±3.94	-1.5±1.45
	R:B:ILE:450	-2.84±7.04	-0.59±3.64	-2.56±1.54
	R:B:PHE:451	-1.29±6.05	-1±2.59	-1.29±1.40
	R:B:VAL:453	-2.44±9.15	-0.49±4.62	-3.2±1.27
	R:B:ARG:466	-3.17±29.3	-147±21.66	0.13±2.35
	R:B:PRO:467	-2.98±5.63	-4.07±2.5	-2.81±1.14

As for the ligand itself (BIK), some residues like PHE:92 (-3.90 kcal/mol) and GLN:79 (-3.23 kcal/mol) were revealed to be the key binding determinants of the R2 system. The existence of such residues, which have not been identified or have been poorly recognized in the R1 system, contributed to the large decrease in the overall binding energy. In terms of therapeutic applications, the determination of these hotspots (in particular, ARG:439 and PHE:92) represents the exact point where drugs may be targeted against the GRP78-BIK complex. Small molecules and peptidomimetics capable of reproducing such interactions would result in effective disruption of this complex, thus facilitating BIK-induced cell death in chemotherapy-resistant breast cancer cells.

Overall, this MM-GBSA study, coupled with per-residue analysis, highlights the importance of taking into account many interactions at the level of individual amino acids when assessing protein-ligand stability.

3.5 Principal Component Analysis and Free Energy Landscape of Regional Conformational Dynamics

When we look at the eigenvalues in the plot, we can see that the two systems are very different when it comes to how flexible they are. The R1 system is an example. The first part, PC1, explains a lot of the variation (42.62 %), while the second part, PC2, explains about 19.12 %. Together, the first two parts explain about 61.75 % of the variation. The R2 system is different. The first part, PC1, only explains about 24.99 % of the variation. The second part, PC2, explains about 15.15 %. So the first two parts only explain about 40.15 % of the variation. It means the R2 system is more stable and compact. It does not change shape much like the R1 system. The extra parts on the R2 system help to make it more stable. They stop the changes that can happen. They make the binding interface more rigid. The R2 system has a restricted conformational space. This is because of the flanking residues in the R2 region. They help to dampen the scale of global fluctuations. The R2 complex is more stable. The R1 and R2 complexes have different behaviors when we look over a long period of time (100 ns).

When we look at the R2 complex, we see that it has stable movements around a certain point, moving between -20 and +20 nm. This shows that the R2 complex is very stable and reaches its shape quickly. On the other hand, the R1 complex has a very different behavior. It starts at -40 nm and moves up to over +60 nm by the end of the time. This big change in the R1 complex means that it is always changing its shape and never settles into one position, especially when the R1 complex is associated with GRP78.

When we look at the trajectory in two dimensions on the PC1 and PC2 subspaces, we can see the same trend because of the colors that change over time in the matrix. The GRP78–R1 complex is over the place, and the different shapes it can be in are really far apart. If we look at the parts of the movement, which are red, they are not near the starting shapes, which are blue. On the other hand, the GRP78–R2 complex is much more compact during the 100 ns simulation. We can see how the protein and the ligand move together and change shape over time when we use PCA.

To provide proof for these results and show the energetics behind this, we created the Free Energy Landscape (FEL) graph for both regions. As it is seen in the FEL plot for R1, the landscape looks extremely open with great distances in PC1 from -40 nm to more than +60 nm and in PC2 from -40 nm to +40 nm. Besides, the stable red zones here are split into independent small areas, thus indicating that R1 is unstable and continuously fluctuates among a variety of conformations. By contrast, in the FEL graph for R2, a much more compact and enclosed structure is revealed. In particular, PC1 here changes from -40 nm to +30 nm, whereas PC2 changes from -30 nm to +30 nm. The red stable areas here are concentrated in one continuous energy well located centrally on this graph. Thus, these results clearly indicate that additional residues in R2 contribute to the rapid and reliable fixation of the complex in its single energy-stable conformational state, as was revealed by PCA trajectories.

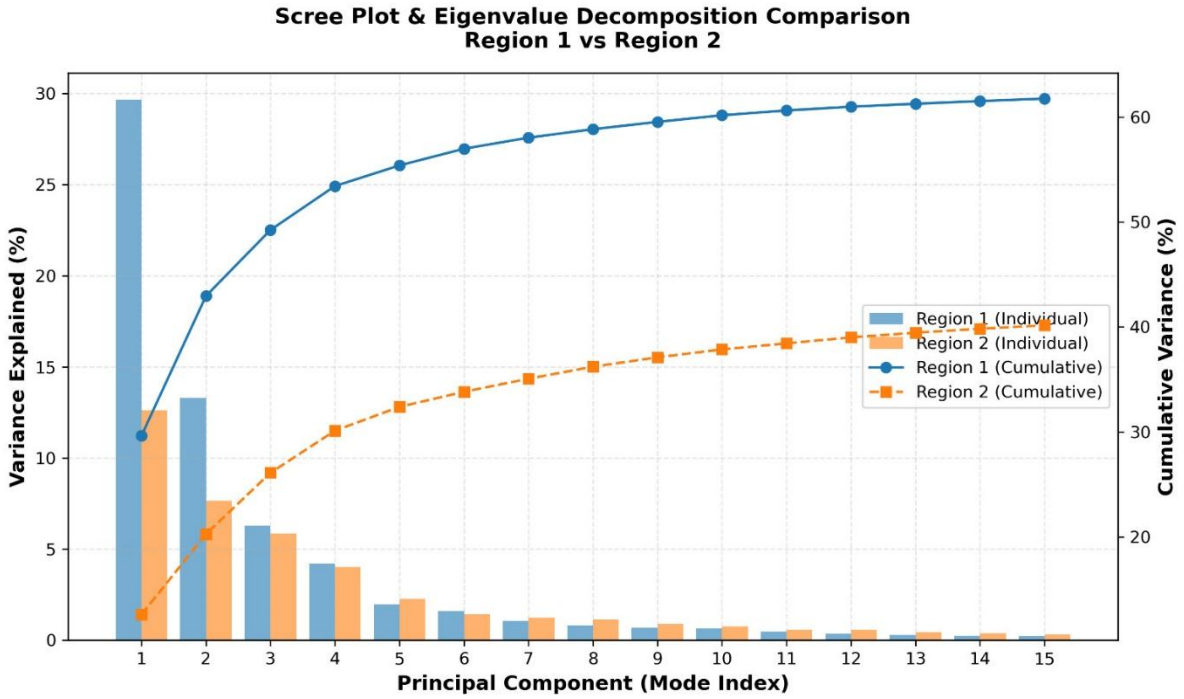


Figure 6: Scree plot and eigenvalue decomposition comparison between GRP78–BIK Region 1 (R1) and Region 2 (R2) complexes over the 100 ns molecular dynamics simulation. The bar chart represents the variance explained by individual principal components (modes 1–15), while the line plots indicate the cumulative variance percentage.

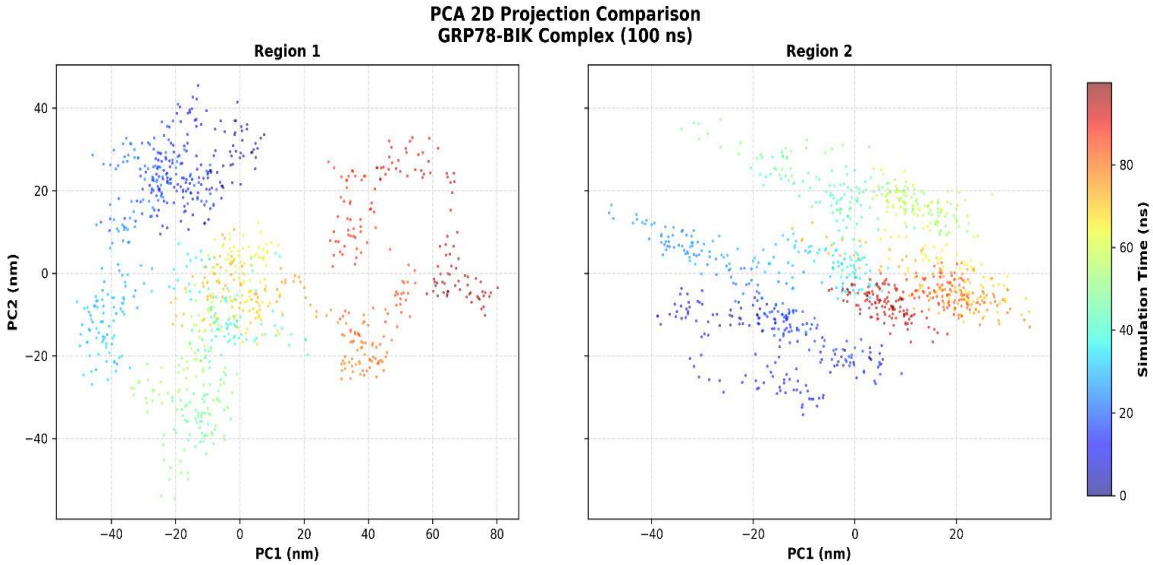


Figure 7 Principal Component Analysis (PCA) 2D projection comparison of GRP78–BIK complexes for Region 1 and Region 2. The trajectories are projected onto the subspace defined by the first two principal components (PC1 vs. PC2) over 100 ns. The color scale gradient from blue to red represents the simulation time evolution from 0 to 100 ns, highlighting the localized structural stability of the R2 complex versus the wide conformational sampling of the R1 complex.

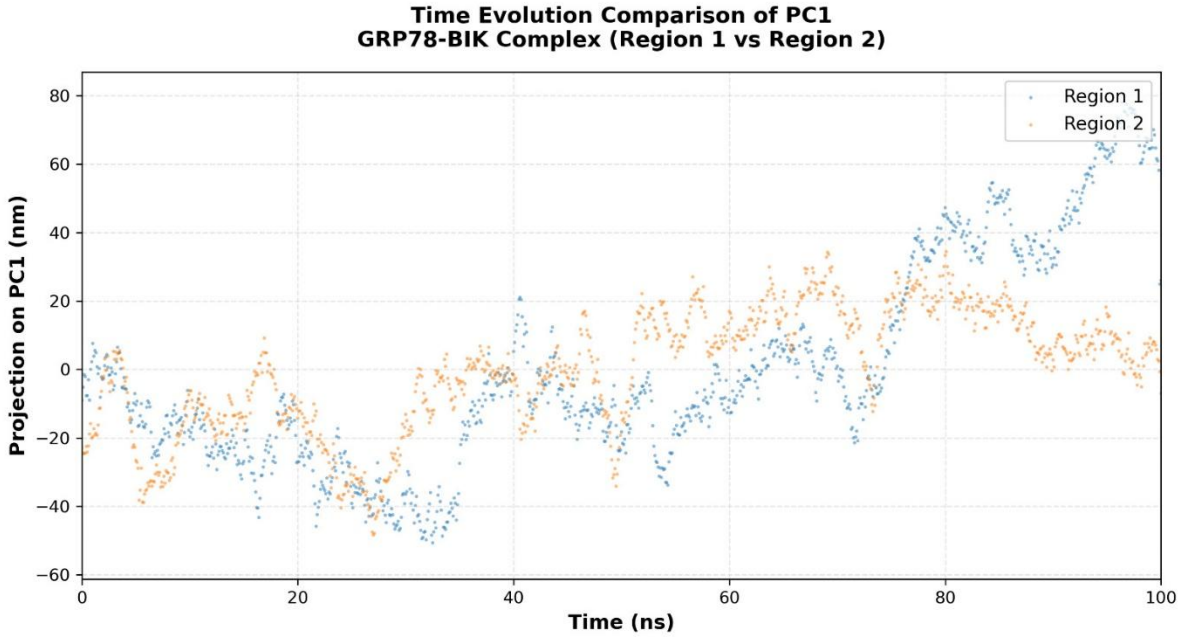


Figure 8:Time evolution of the projection of trajectories onto the first principal component (PC1) for the GRP78–BIK Region 1 (blue) and Region 2 (orange) complexes across the entire 100 ns production run. The plot illustrates the contrasting conformational transitions and equilibrium convergence behaviors of both systems.

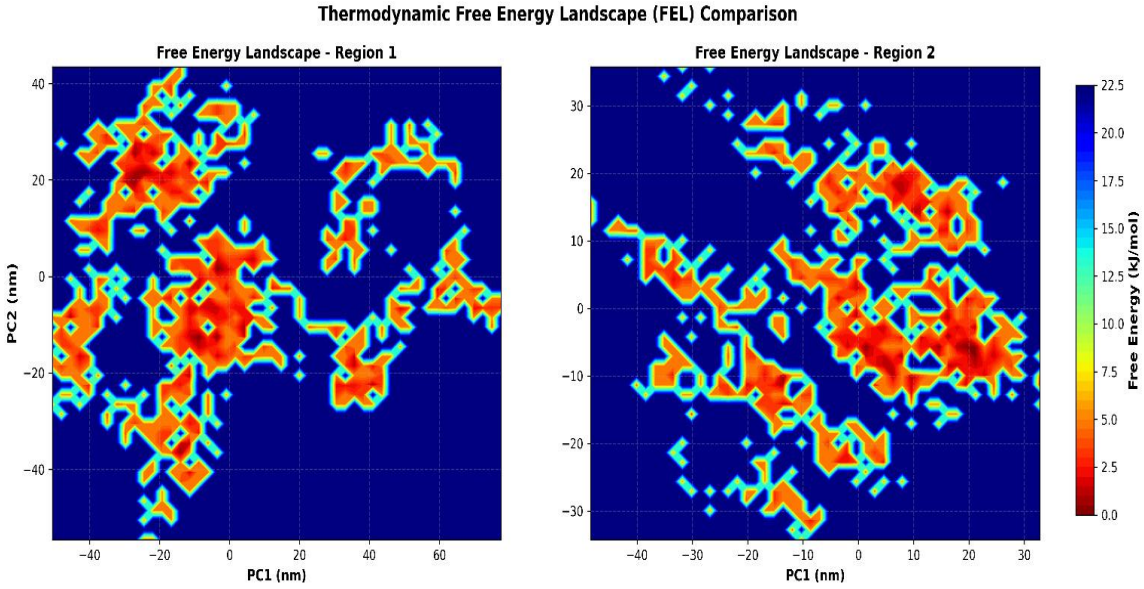


Figure 9 Free Energy Landscape (FEL) plots of GRP78 complexes during a 100 ns molecular dynamics simulation. GRP78–R1 complex showing a wide, scattered conformational sampling with multiple local energy minima. GRP78–R2 complex showing a highly compact and centralized deep energy well. The color bar on the right represents the free energy values in kJ/mol, where red regions indicate the lowest energy states (most stable conformations) and blue regions indicate the highest energy states.

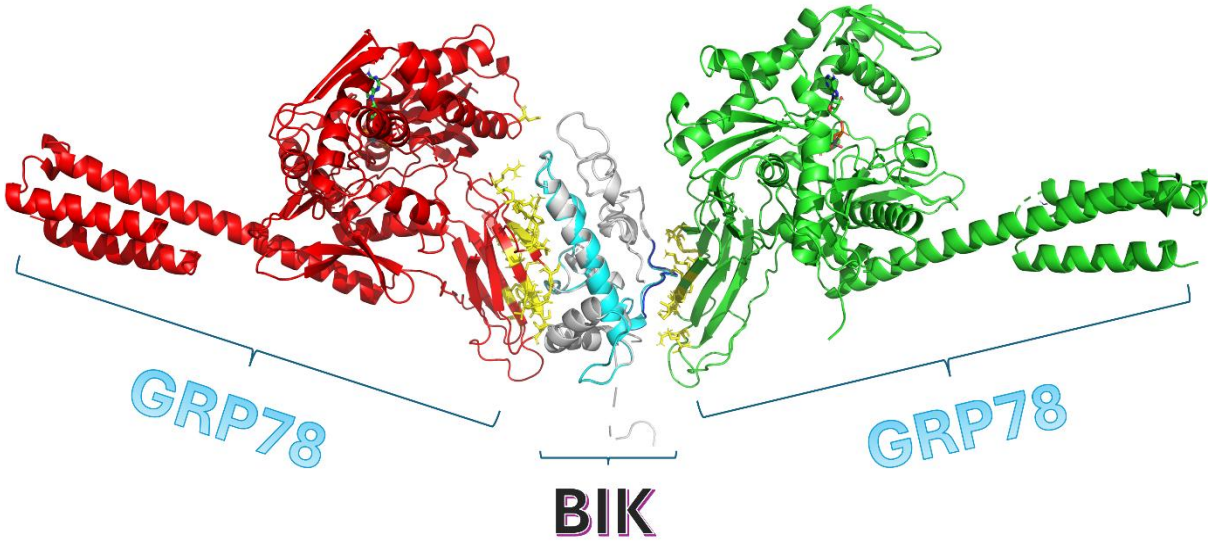


Figure 10 The superposition of the two complexes of BIK at R1 (right) (shown in blue cartoon) and R2 (left) (cyan cartoon) with GRP78. Yellow sticks are the interacting residues from GRP78 in both complexes.

3.6. Interfacial Stability and Dynamic Coordination Analysis

To examine the stability of the GRP78-BIK complex structure over time and the synchronization of their movements, an interfacial hydrogen bond analysis and Dynamic Cross-Correlation Matrix calculation were performed.

3.6.1. Hydrogen Bond Dynamics and Salt-Bridge Stability

The stability of the GRP78-BIK complexes relies mainly on the large network of polar interactions. As seen from Table 5, the BIK_R2 complex has a more favorable hydrogen bond pattern than R1 in terms of greater persistence and optimal geometry. The crucial point is that the formation of a stable salt bridge between ARG439 and ASP95 has been found, with an excellent occupancy rate of 98% throughout the entire 100ns simulation period. This interaction serves as a "structural anchor" that prevents the peptide BIK from detaching from the GRP78 binding site and makes it resistant to thermal perturbations.

The significance of the Arginine residues in stabilizing the complex structure can be seen from the consistency between MM-GBSA binding scores and occupancy rates. Interestingly, the residue with the highest per-residue energetic contribution (ARG439, see Table 4) is the same residue that participates in the persistent salt bridge with ASP95 described above (98% occupancy). This residue also serves a dual stabilizing role at the R2 interface, providing the largest single energetic contribution to the binding free energy and the most persistent structural interaction of the complex, thereby designating it as the principal molecular anchor of the R2 interface. In particular, ARG439 has the largest single electrostatic term of all residues in the interface (see Table 4). In these same metrics, a

second different arginine residue is found consistently directly behind ARG439. ARG466 has the second highest total binding energy, the second highest electrostatic contribution, and the second most persistent hydrogen bond of the interface with ASP99 (55% occupancy rate). Another relatively minor interaction, SER47-MET433 (with an occupancy rate of 55.86%), was also observed in R1.

On the ligand (BIK) side of the interface, PHE92 and GLN79 were the two strongest energetic contributors with total binding energies of -3.90 and -3.23 kcal/mol, respectively (see Table 4), comparable to ARG466 on the GRP78 side. In particular, the physical basis of their stabilizing contribution is markedly different from the GRP78-side arginine hotspots: while ARG439 and ARG466 are dominated by favorable electrostatic interactions consistent with salt-bridge formation, both PHE92 and GLN79 exhibit net unfavorable electrostatic terms that are compensated by strongly favorable van der Waals contributions (-2.50 and -3.45 kcal/mol, respectively). This suggests that PHE92 and GLN79 are involved in stabilizing the R2 interface mainly by hydrophobic packing and not by electrostatic complementarity, in addition to the electrostatically driven anchoring of the GRP78-side arginine residues.

Table 5: Hydrogen bond and salt-bridge occupancy at the GRP78-BIK interface. The R2 complex displays exceptionally stable interactions, notably the ARG439-ASP95 salt-bridge with 98% occupancy.

	Donor Residue	Acceptor Residue	Occupancy%	Interaction Type	Stability
R1_Complex	SER47	MET433	55.86	H-bond	High
	LYS435	ASP46	53.75	H-bond	High
	ARG466	GLU28	52.85	H-bond	High
	ARG488	LYS160	44.84	H-bond	Moderate high
R2_Complex	ARG439	ASP95	98	Salt Bridge	Very high
	ARG466	ASP99	55	H-bond	High
	ARG76	GLU494	40.4	H-bond	High

The hydrogen bond distance distribution (Figure 11) supports these observations, showing a sharper, more intense probability density peak for R2 at shorter distances (< 0.30 nm) compared to R1. Additionally, the angle distribution (Figure 8) confirms that R2 maintains more geometrically favorable bond orientations (peaking near 10-15°), ensuring maximum orbital overlap and bond strength.

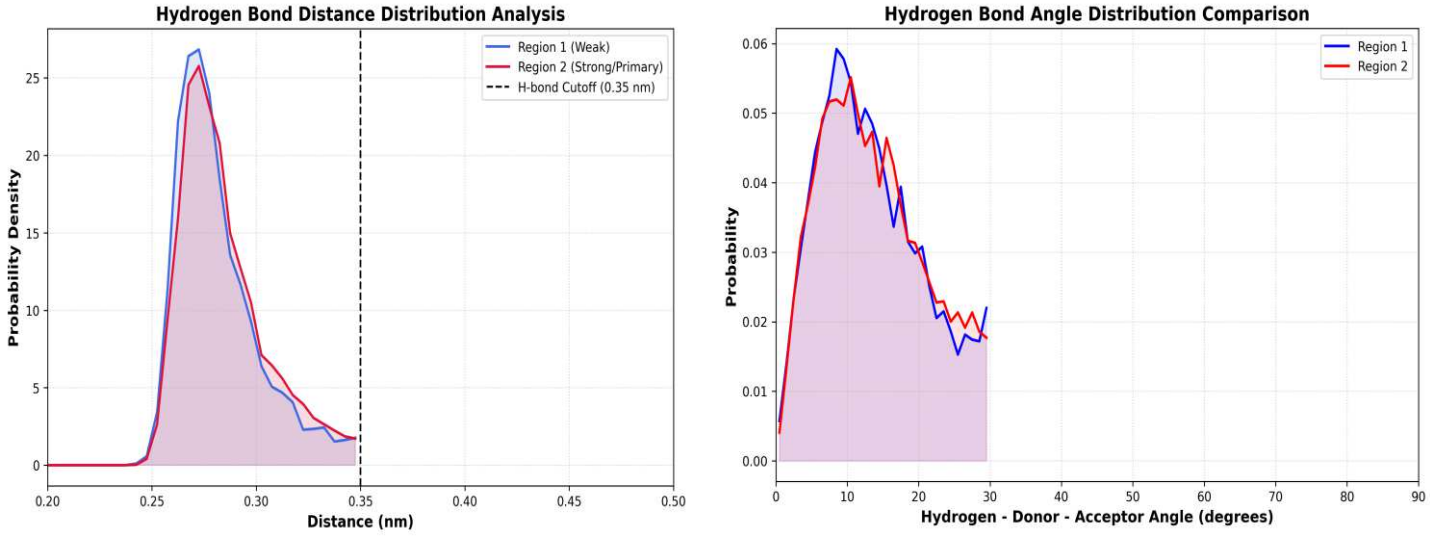


***Figure 11**: Hydrogen bond distance and angle distribution analysis. The sharper probability peaks for region 2 indicate more stable and geometrically favorable binding contacts.*

3.6.2. Dynamic Cross-Correlation Matrix (DCCM) Analysis

Dynamic Cross-Correlation Matrix (DCCM) analysis was performed to investigate the correlated movements of the residues from the BIK and GRP78 proteins. Heatmaps obtained through the analysis (Figure 12A) reveal a distinct difference in the correlated dynamics. Specifically, the BIK_R2–GRP78 complex (Figure 9B) exhibits a significantly stronger and structured correlation pattern (cyan/blue areas) compared to the R1 system. These observations imply that the R2 site and GRP78 SBD constitute a functional unit that moves synchronously. The formation of a robust salt bridge network, particularly with the arginines mentioned above, facilitates a strong coupling of the ligand with the receptor, thus preventing spontaneous and unpredictable movements of the receptor. All of the aforementioned results strongly suggest that the R2 domain fosters a more unified interaction that is necessary for GRP78 inhibition.

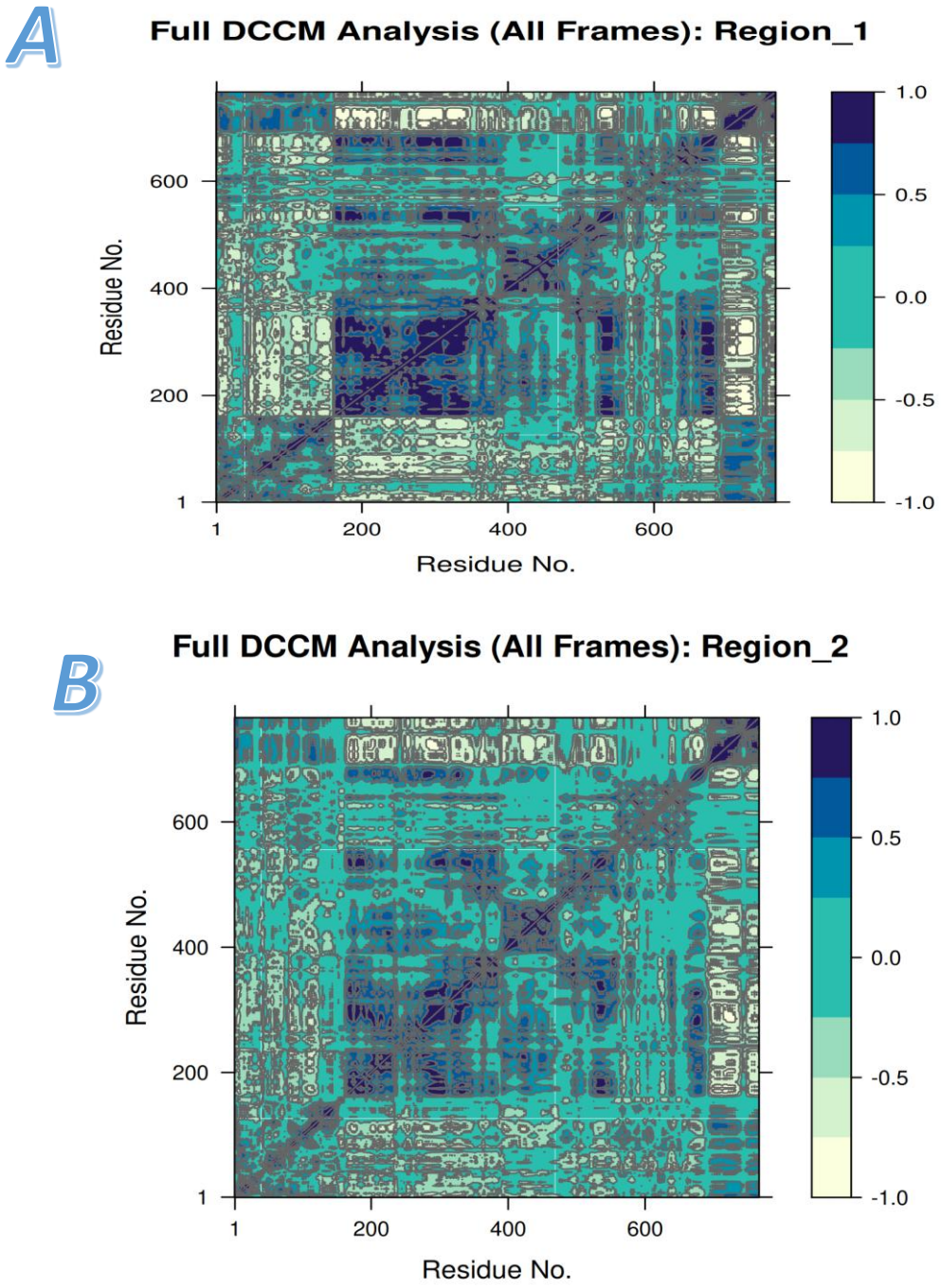


***Figure 12**: Dynamic cross-correlation matrix (DCCM) of (A) region 1 and (B) region 2 complexes. The more prominent cyan regions in R2 signify highly synchronized and correlated motions between the ligand and receptor.*

Conclusion

In this study, an attempt was made to present a detailed and robust molecular analysis of the GRP78-BIK interaction, an important complex responsible for apoptosis escape in endocrine-resistant breast cancer. The current paper presents fundamental

information about the structural details of the functional complex that may serve as the ground for further research on drug design.

Firstly, a series of computationally based methods was used, which included homology studies followed by rigid-body docking using HADDOCK v2.4. The preliminary results highlighted Region 1 (R1: residues 50-63) because of the sequence similarity to the Pep42 binder and good docking score values. However, the integration of MDS performed for 100 ns and carried out using NAMD software with the CHARMM36 force field required a revision of the preferred mode of binding. According to RMSD/RMSF/SASA/RoG graphs, the dynamics proved to be stable for both binding modes. Besides, in favor of the R2_GRP78 complex, a more negative binding free energy value was shown as the result of MM-GBSA (R2: -50.92 ± 12.19 kcal/mol; R1: -31.54 ± 15.90 kcal/mol).

An important molecular property of the studied complex is that of a multi-functional binding site at the interface of Region 2. Using the per-residue energy values, a single arginine residue, ARG439, was recognized as the main anchor of the R2 interface, as it is the highest single energy binder contributing more than 10 kcal/mol to the total binding energy, while hydrogen bond analysis revealed that ARG439 forms a permanent salt bridge with ASP95 (occupancy rate 98%), acting as the structural anchor of the interface. Thus, being both the strongest energy and the most persistent structural contributor to the binding process makes ARG439 the key player in maintaining the stability of the R2 interface. A secondary arginine residue, ARG466, also provides stabilization through the second highest contribution to the electrostatics of the interface and the second most persistent hydrogen bond (occupancy rate 55% with ASP99). From the BIK side of the interface, PHE92 and GLN79 were found to contribute the highest to the total energy of the binding (-3.90 and -3.23 kcal/mol, respectively), being responsible for the van der Waals packing.

Dynamic differences in this system were found based on principal component analysis and DCCM results. In fact, from the analysis, it appeared that both systems had a stable core, but the R2 system had a different correlation pattern than that of R1, which signifies a more dynamically coupled interface. This can be observed from the PCA scree plot and 2D projection (Figure 6&Figure 7) and free energy landscape (Figure 9), and a higher level of cross-correlation between the ligand and GRP78 receptor in the DCCM (Figure 12). It fits well with the idea of an adaptive interface in R2 since there is much higher correlation between ligand and receptor movements, the accessible conformational subspace becomes significantly smaller (R2: 40.15% vs. R1: 61.75% of variance explained

by the first two principal components – that is, the motion pattern is less diffuse), and the whole complex finds itself in one unique, thermodynamically favorable energy minimum rather than on a widely dispersed multi-minima energy landscape like R1. This convergence of results provides support for considering the binding site in question as an adaptive interface. However, identification of the exact nature of adaptivity (induced fit or conformational selection) will require additional experimental data, such as comparing apo- and holo-complexes.

From a clinical perspective, this means that the disruption of this dynamic interface can be considered a promising target for the disengagement of BIK. It is likely that by disrupting the connection of GRP78 with BIK, it will be possible to reactivate apoptosis in endocrine-resistant tumors. Specifically, the structural insights obtained from the hot-spot residues and the rigid binding interface found in R2 can directly guide future drug design. To advance this therapeutic strategy, future work will focus on performing *in silico* alanine scanning mutagenesis on these identified hot-spot residues. This next step will precisely quantify their individual energetic contributions to the interface stability, thereby providing a definitive structural template for designing targeted small-molecule inhibitors or peptidomimetics to overcome breast cancer chemoresistance.

Overall, this study provides a molecular blueprint for targeting the GRP78-BIK interface, offering a strategic foundation for developing small-molecule inhibitors to overcome endocrine resistance in breast cancer.

Acknowledgment

We acknowledge Bibliotheca Alexandrina and Fayoum University for providing the HPC for the MDS calculations.

CRediT author contributions statement

A.E. led the research activity planning, execution, data analysis, graphics, and revised the manuscript. **N.A.** performed the *in silico* studies, calculations, and analysis of the results, and wrote the manuscript. **Y.E.** revised the manuscript. **Y.M.** contributed by setting up the computational environment for molecular dynamics simulations—including installing Rocky Linux, integrating NAMD with NVIDIA GPU acceleration, preparing the system for high-performance computing, and revising the manuscript. **A.E., Y.E,** and **Y.M.** supervised **N.A.** All authors reviewed and approved the final version of the manuscript.

DECLARATIONS

Funding: N/A

Conflict of Interest: None.

Ethical approval: The work did not include any animals or human participants.

Consent to publish: The Authors give consent to publish the manuscript.

Data availability: Data available upon request from the authors.

Competing interests: All authors declare that they have no known competing financial interests or personal relationships that could have appeared to influence the work reported in this paper.

References

[1] A. Kawiak, A. Domachowska, A. Jaworska, and E. Lojkowska, "Plumbagin sensitizes breast cancer cells to tamoxifen-induced cell death through GRP78 inhibition and Bik upregulation," *Sci. Rep.*, vol. 7, 2017, doi: 10.1038/s41598-017-04620-3.

[2] Lu B, N.E., Balaji Raghavendran HR, and Markandan UD, "Molecular Classification, Treatment, and Genetic Biomarkers in Triple-Negative Breast Cancer," *Technol. Cancer Res. Treat.*, vol. 22, 2023, doi: 10.1177/15330338231184351.

[3] Y. Liu and e.a, "Advances in immunotherapy for triple-negative breast cancer," *Mol. Cancer*, vol. 22, no. 1, pp. 1–27, 2023, doi: 10.1186/s12943-023-01850-w.

[4] H. Zhou, Y. Zhang, Y. Fu, L. Chan, and A. S. Lee, "Novel Mechanism of Anti-apoptotic Function of 78-kDa Glucose-regulated Protein (GRP78): Isolation and Characterization of GRP78-binding Peptides," *Journal of Biological Chemistry (JBC)*, vol. 286, no. 17, pp. 14713–14725, 2011.

[5] Y. Fu, J. Li, and A. Lee, "GRP78/BiP inhibits endoplasmic reticulum BIK and protects human breast cancer cells against estrogen starvation–nduced apoptosis.," *Cancer Research*, vol. 67, no. 8, pp. 3734–3740, 2007, doi: 10.1158/0008-5472.CAN-06-4594.

[6] Ruiz Esparza-Garrido *et al.*, "Accurate identification of BIK binding sites at the MDA-MB-231 cell genome by human tiling arrays," *Cancer Biology and Therapeutic Oncology*, 2018.

[7] M. Germain and G. C. Shore, “BIK, the founding member of the BH3-only family proteins: mechanisms of cell death and role in cancer,” *Oncogene*, vol. 28, no. S1, pp. S20–S29, 2009, doi: 10.1038/onc.2009.43.

[8] Martínez-García, R. González-González, and M, “ Expression changes of BIK in breast cancer tissues of different histological subtypes,” *Cirugía y Cirujanos*, vol. 88, no. 2, pp. 163–170, 2020, doi: CIRU.19000854/10.24875.

[9] R. Ruiz-Esparza-Garrido, J. Torres-López, P. Piña-Sánchez, R. Viedma-Rodríguez, A. Rivera-González, and M. A. Velázquez-Flores, “Expression changes of BIK in breast cancer tissues of different histological subtypes,” *Cir. Cir.*, vol. 88, no. 2, pp. 163–171, Feb. 2020, doi: 10.24875/CIRU.19001039.

[10] J. P. Mathai, M. Germain, and G. C. Shore, “BIK regulates mitochondrial function and apoptosis in cells,” *Oncogene*, vol. 21, no. 17, pp. 2534–2544, 2002, doi: org/10.1038/sj.onc.1205634.

[11] J. M. Boyd, S. Malstrom, T. Subramanian, and et al, “BIK, a novel death-inducing protein shares a domain with BCL-2 family proteins,” *Oncogene*, vol. 11, no. 9, pp. 1921–1928, 1995, Accessed: Apr. 10, 2026. [Online]. Available: https://pubmed.ncbi.nlm.nih.gov/7478510

[12] X. Chen, J. Lee, and H. Wang, “Bik promotes apoptosis by activating Bak and Bax in response to endoplasmic reticulum stress,” *Oncogene*, vol. 38, no. 10, pp. 1664–1674, 2019, doi: s41388-018-0524-7.

[13] S. J. Korsmeyer and et al, “ Pro-apoptotic members of the Bcl-2 family regulate mitochondrial function,” *Current Biology*, vol. 3, no. 5, pp. 290–295, 1993, doi: org/10.1016/S0960-9822(93)90119-X.

[14] Willis, S.N, and et al, “ Apoptosis mediated by BIK through mitochondrial outer membrane permeabilization,” *Genes Dev.*, vol. 21, no. 11, pp. 1339–1353, 2007, doi: 10.1101/gad.1507107.

[15] J. M. Adams and S. Cory, “ The Bcl-2 apoptotic switch in cancer development and therapy ,” *Nat. Rev. Cancer*, vol. 7, no. 9, pp. 711–722, 2007.

[16] S. Rajan and et al, “ BIK silencing in breast cancer via promoter hypermethylation,” *Experimental Cell Research*, vol. 317, no. 15, pp. 2118–2124, 2011, doi: 10.1016/j.yexcr.2011.05.011.

[17] M. T. Cervantes-Díaz *et al.*, " BIK and GRP78 protein expression as possible markers of response to preoperative chemotherapy and survival in breast cancer," *Taiwan. J. Obstet. Gynecol.*, vol. 60, no. 5, pp. 849–856, 2021, doi: 10.1016/j.tjog.2021.07.014.

[18] I. M. Ibrahim, D. H. Abdelmalek, and A. A. Elfiky, "GRP78: A cell's response to stress," *Life Sci.*, vol. 226, pp. 156–163, Jun. 2019, doi: 10.1016/j.lfs.2019.04.022.

[19] A. S. Lee, "Glucose-regulated proteins in cancer: therapeutic implications," *Curr. Opin. Cell Biol.*, vol. 27, pp. 123–129, 2014, doi: 10.1016/j.ceb.2013.12.001.

[20] J. Li and A. S. Lee, "Stress-inducible GRP78 as a potential cancer therapeutic target. ," *Mol. Oncol.*, vol. 1, no. 1, pp. 3–12, 2006, doi: 10.1016/j.molonc.2006.05.006.

[21] J. Zhang and B. Zhang, "The multifaceted role of GRP78/BiP in tumor microenvironment and therapeutic resistance. ," *Front. Oncol.*, vol. 12, 2022, doi: 10.3389/fonc.2022.1001484.

[22] Y. Fu, J. Li, and A. S. Lee, " GRP78/BiP is a novel downstream target of IGF-1 receptor signaling and promotes breast cancer growth and metastasis," *Cancer Res.*, vol. 67, no. 8, pp. 3701–3710, 2007, doi: 10.1158/0008-5472.CAN-07-0461.

[23] R. K. Reddy, C. Mao, P. Baumeister, and et al, " ndoplasmic reticulum chaperone protein GRP78 protects cells from apoptosis induced by topoisomerase inhibitors," *Journal of Biological Chemistry*, vol. 278, no. 23, pp. 20915–20924, 2003, doi: 10.1074/jbc.M212328200.

[24] Y. Fu and et al, " GRP78 suppression of apoptosis and modulation of BIK function. ," *Cancer Cell*, vol. 67, no. 8, pp. 3701–3710, 2008, doi: 10.1158/0008-5472.CAN-07-0461.

[25] S. Rao and et al, "GRP78 modulation of apoptosis and its role in breast cancer.," *Mol. Oncol.*, vol. 12, no. 12, pp. 2041–2051, 2018, doi: 10.1002/1878-0261.12320.

[26] A. A. Elfiky, Kirolos R. Mansour, Yousef Mohamed, Yomna Kh. Abdelaziz, and Ian A. Nicholls, " Exploring the Anticancer Potential of Proton Pump Inhibitors by Targeting GRP78 and V-ATPase: Molecular Docking, Molecular Dynamics, PCA, and MM-GBSA Calculations.," *International Journal of Molecular Sciences*, vol. 26, no. 1, 2025.

[27] M. E. Rashwan, M. R. Ahmed, and A. A. Elfiky, " In silico prediction of GRP78-CRIPTO binding sites to improve therapeutic targeting in glioblastoma," *Sci. Rep.*, vol. 15, 2025.

[28] L. A. Kelley and M. J. E. Sternberg, "Protein structure prediction on the Web: a case study using the Phyre server," *Nat. Protoc.*, vol. 4, no. 3, pp. 363–371, Mar. 2009, doi: 10.1038/nprot.2009.2.

[29] J. Jumper *et al.*, "Highly accurate protein structure prediction with AlphaFold," *Nature*, vol. 596, no. 7873, pp. 583–589, Aug. 2021, doi: 10.1038/s41586-021-03819-2.

[30] J. Yang, R. Yan, and A. Roy, "The I-TASSER Suite: protein structure and function prediction," *Nat. Protoc.*, vol. 10, no. 1, pp. 155–173, 2015.

[31] C. J. Williams *et al.*, "MolProbity: More and better reference data for improved all-atom structure validation," *Protein Science*, vol. 27, no. 1, pp. 293–315, Jan. 2018, doi: 10.1002/pro.3330.

[32] G. Chinnadurai, S. Vijayalingam, and R. Rashmi, " BIK, the founding member of the BH3-only family proteins: mechanisms of cell death and role in cancer and pathogenic processes," *Oncogene*, vol. 27, no. S1, pp. S20–S29, 2009.

[33] A. Bateman *et al.*, "UniProt: the universal protein knowledgebase in 2021," *Nucleic Acids Res.*, vol. 49, no. D1, pp. D480–D489, Jan. 2021, doi: 10.1093/nar/gkaa1100.

[34] Y. Kim et al, "Targeting heat shock proteins on cancer cells: selection, characterization, and cell-penetrating properties of a peptidic GRP78 ligand," *Biochemistry*, vol. 45, pp. 9434–9444, 2006.

[35] D. G. Youssef, H. I. A. Mostafa, A. H. Faraag, and A. A. Elfiky, "Computational investigation of the interplay between cellular stress and ferroptosis in triple-negative breast cancer," *Pathol. Res. Pract.*, vol. 271, p. 156008, Jul. 2025, doi: 10.1016/j.prp.2025.156008.

[36] F. Madeira *et al.*, "The EMBL-EBI Job Dispatcher sequence analysis tools framework in 2024," *Nucleic Acids Res.*, vol. 52, no. W1, pp. W521–W525, Jul. 2024, doi: 10.1093/nar/gkae241.

[37] V. K. Garg *et al.*, "MFPPI–multi FASTA ProtParam interface," *Bioinformation*, vol. 12, no. 11, pp. 584–587, 2016.

[38] A. A. Elfiky, I. M. Ibrahim, and A. M. Elgohary, “SARS-CoV-2 Delta Variant is Recognized Through GRP78 Host-Cell Surface Receptor, In Silico Perspective,” *Int. J. Pept. Res. Ther.*, vol. 28, no. 5, p. 146, Aug. 2022, doi: 10.1007/s10989-022-10450-w.

[39] S. Jo, T. Kim, V. G. Iyer, and W. Im, “CHARMM-GUI: A web-based graphical user interface for CHARMM,” *J. Comput. Chem.*, vol. 29, no. 11, pp. 1859–1865, Aug. 2008, doi: 10.1002/jcc.20945.

[40] S. Jo, X. Cheng, and S. M. Islam, “CHARMM-GUI PDB manipulator for advanced modeling and simulations of proteins containing nonstandard residues,” *Adv. Protein Chem. Struct. Biol.*, vol. 96, pp. 235–265, 2014.

[41] J. Lee *et al.*, “CHARMM-GUI Input Generator for NAMD, GROMACS, AMBER, OpenMM, and CHARMM/OpenMM Simulations Using the CHARMM36 Additive Force Field,” *J. Chem. Theory Comput.*, vol. 12, no. 1, pp. 405–413, Jan. 2016, doi: 10.1021/acs.jctc.5b00935.

[42] W. Humphrey, A. Dalke, and K. Schulten, “VMD: Visual molecular dynamics,” *J. Mol. Graph.*, vol. 14, no. 1, pp. 33–38, Feb. 1996, doi: 10.1016/0263-7855(96)00018-5.

[43] I. Khater and A. Nassar, “SARS-CoV-2 variant surge and vaccine breakthrough infection: A computational analysis,” *Inform. Med. Unlocked*, vol. 29, p. 100873, 2022, doi: 10.1016/j.imu.2022.100873.

[44] I. M. Ibrahim, D. H. Abdelmalek, and A. A. Elfiky, “COVID-19 spike-host cell receptor GRP78 binding site prediction,” *J. Med. Virol.*, vol. 92, no. 9, pp. 1554–1560, 2020.

[45] E. C. Meng *et al.*, “<scp>UCSF ChimeraX</scp> : Tools for structure building and analysis,” *Protein Science*, vol. 32, no. 11, Nov. 2023, doi: 10.1002/pro.4792.

[46] R. V. Honorato *et al.*, “The HADDOCK2.4 web server for integrative modeling of biomolecular complexes,” *Nat. Protoc.*, vol. 19, no. 11, pp. 3219–3241, Nov. 2024, doi: 10.1038/s41596-024-01011-0.

[47] L. C. Xue, J. P. Rodrigues, P. L. Kastritis, A. M. Bonvin, and A. Vangone, “PRODIGY: a web server for predicting the binding affinity of protein–protein complexes,” *Bioinformatics*, vol. 32, no. 23, pp. 3676–3678, Dec. 2016, doi: 10.1093/bioinformatics/btw514.

[48] A. Vangone and A. M. Bonvin, “Contacts-based prediction of binding affinity in protein–protein complexes,” *Elife*, vol. 4, Jul. 2015, doi: 10.7554/eLife.07454.

[49] M. F. Adasme *et al.*, “PLIP 2021: expanding the scope of the protein–ligand interaction profiler to DNA and RNA,” *Nucleic Acids Res.*, vol. 49, no. W1, pp. W530–W534, 2021.

[50] S. Yuan, H. C. S. Chan, and Z. Hu, “Using <scp>PyMOL</scp> as a platform for computational drug design,” *WIREs Computational Molecular Science*, vol. 7, no. 2, Mar. 2017, doi: 10.1002/wcms.1298.

[51] S. Genheden and U. Ryde, “The MM/PBSA and MM/GBSA methods to estimate ligand-binding affinities,” *Expert Opin. Drug Discov.*, vol. 10, no. 5, pp. 449–461, May 2015, doi: 10.1517/17460441.2015.1032936.

[52] T. Hou, J. Wang, Y. Li, and W. Wang, “Assessing the Performance of the MM/PBSA and MM/GBSA Methods. 1. The Accuracy of Binding Free Energy Calculations Based on Molecular Dynamics Simulations,” *J. Chem. Inf. Model.*, vol. 51, no. 1, pp. 69–82, Jan. 2011, doi: 10.1021/ci100275a.

[53] J. Chen, J. Wang, W. Wang, L. Zhao, H. Jin, and G. Hu, “Molecular mechanism underlying conformations and region communications of periplasmic receptor affected by diversity of phosphate groups,” *Int. J. Biol. Macromol.*, vol. 361, p. 151977, May 2026, doi: 10.1016/j.ijbiomac.2026.151977.

[54] Chen *et al.*, “ Allosteric binding-mediated suppression on activity of G12D KRAS recognized via markov state model and communication pathway.,” *The Journal of Physical Chemistry B*, 2026.

[55] E. N. Baker and R. E. Hubbard, “Hydrogen bonding in globular proteins,” *Prog. Biophys. Mol. Biol.*, vol. 44, no. 2, pp. 97–179, 1984, doi: 10.1016/0079-6107(84)90007-5.

[56] B. J. Grant, A. P. C. Rodrigues, K. M. ElSawy, J. A. McCammon, and L. S. D. Caves, “Bio3d: an R package for the comparative analysis of protein structures,” *Bioinformatics*, vol. 22, no. 21, pp. 2695–2696, Nov. 2006, doi: 10.1093/bioinformatics/btl461.

[57] T. Ichiye and M. Karplus, “Collective motions in proteins: A covariance analysis of atomic fluctuations in molecular dynamics and normal mode simulations,” *Proteins:*

Structure, Function, and Bioinformatics, vol. 11, no. 3, pp. 205–217, Nov. 1991, doi: 10.1002/prot.340110305.

[58] G. A. Jeffrey, *An introduction to hydrogen bonding.* . Oxford University Press, 1997.

[59] A. S. Lee, "The ER chaperone and signaling regulator GRP78/BiP as a monitor of endoplasmic reticulum stress," *Methods*, vol. 35, no. 4, pp. 373–381, 2005.

[60] J. D. Malhotra and R. J. Kaufman, "The endoplasmic reticulum and the unfolded protein response," *Semin. Cell Dev. Biol.*, vol. 18, no. 6, pp. 716–731, 2007.

[61] G. Gazit, J. Lu, and A. S. Lee, "De-regulation of GRP stress protein expression in human breast cancer cell lines," *Breast Cancer Res. Treat.*, vol. 54, no. 2, pp. 135–146, 1999.

[62] E. Lee, P. Nichols, and D. Spicer, "GRP78 as a Novel Predictor of Responsiveness to Chemotherapy in Breast Cancer," *Cancer Res.*, vol. 66, no. 16, pp. 7849–7853, 2006.

[63] M. A. Arap *et al.*, "Cell surface expression of the stress response chaperone GRP78 enables tumor targeting by circulating ligands," *Cancer Cell*, vol. 6, no. 3, pp. 275–284, Sep. 2004, doi: 10.1016/j.ccr.2004.08.018.

[64] V. Ekberg and U. Ryde, "On the Use of Interaction Entropy and Related Methods to Estimate Binding Entropies," *J. Chem. Theory Comput.*, vol. 17, no. 8, pp. 5379–5391, Aug. 2021, doi: 10.1021/acs.jctc.1c00374.